ERDC/GSL TR-18-1

US Army Corps
of Engineers®
Engineer Research and
Development Center

ERDC
INNOVATIVE SOLUTIONS
for a safer, better world

Performance Prediction Relationships for AM2 Airfield Matting Developed from Full-Scale Accelerated Testing and Laboratory Experimentation

Timothy W. Rushing

January 2018

Geotechnical and Structures Laboratory

The U.S. Army Engineer Research and Development Center (ERDC) solves the nation's toughest engineering and environmental challenges. ERDC develops innovative solutions in civil and military engineering, geospatial sciences, water resources, and environmental sciences for the Army, the Department of Defense, civilian agencies, and our nation's public good. Find out more at www.erdc.usace.army.mil.

To search for other technical reports published by ERDC, visit the ERDC online library at http://acwc.sdp.sirsi.net/client/default.

ERDC/GSL TR-18-1
January 2018

Performance Prediction Relationships for AM2 Airfield Matting Developed from Full-Scale Accelerated Testing and Laboratory Experimentation

Timothy W. Rushing

Geotechnical and Structures Laboratory
U.S. Army Engineer Research and Development Center
3909 Halls Ferry Road
Vicksburg, MS 39180-6199

Final report

Prepared for U.S. Air Force Civil Engineer Center
Tyndall AFB, FL 32403-5319

Under Demonstration Project 6.3, "Port of Debarkation, Assess and Upgrade"

Abstract

The AM2 airfield matting system is used by the U.S. military for temporary, rapidly constructed airfields. Predicting the number of allowable aircraft passes across an AM2 installation is challenging because of the complex design of the joining system and the fatigue behavior of the joints. Prior to this work, the prevailing methods used to predict the performance of AM2 were based on the CBR design procedure for flexible pavements using a small number of full-scale test sections over CBRs ranging from 4 to 10 percent and simulated aircraft that are no longer in service. This report presents results from nine full-scale experiments conducted on sections of AM2 matting installed on unstabilized soil and gravel subgrades with CBRs of 6, 10, 15, 25, and 100 percent, and provides improved relationships for predicting subgrade deformation underneath an AM2 mat installation and the associated fatigue damage when subjected to F-15E and C-17 traffic. Additionally, a laboratory fixture and procedure is described for evaluating an AM2 style joint in fatigue and relating its performance to given field conditions without requiring the expense of full-scale testing. These relationships are suitable for design and evaluation frameworks currently used for airfield pavements and matting systems.

Contents

Figures and Tables

Figures

Tables

Preface

This study was a compilation of projects conducted for the U.S. Air Force Civil Engineer Center (AFCEC) under the Rapid Parking Ramp Expansion and the Airfield Damage Repair Modernization programs and the U.S. Army Assistant Secretary of the Army for Acquisition, Logistics, and Technology under the 6.3 demonstration project, "Port of Debarkation, Assess and Upgrade (POD A&U)." The technical monitors were Dr. Craig Rutland of AFCEC and Mr. Nicholas Boone of the ERDC.

The work was performed by the Airfields and Pavements Branch (APB) of the Engineering Systems and Materials Division (ESMD), U.S. Army Engineer Research and Development Center, Geotechnical and Structures Laboratory (ERDC-GSL). At the time of publication, Dr. Timothy W. Rushing was Chief, APB; Dr. Gordon W. McMahon was Chief, ESMD; and Mr. Nicholas Boone was the Technical Director for Force Projection and Maneuver Support. The Acting Deputy Director of ERDC-GSL was Mr. Charles W. Ertle, and the Director was Mr. Bartley P. Durst.

COL Bryan S. Green was the Commander of ERDC, and Dr. David W. Pittman was the Director.

Unit Conversion Factors

Multiply	By	To Obtain
degrees (angle)	0.01745329	radians
degrees Fahrenheit	(F-32)/1.8	degrees Celsius
feet	0.3048	meters
inches	0.0254	meters
inch-pounds (force)	0.1129848	newton meters
pounds (force)	4.448222	newtons
pounds (force) per sqft	47.88026	pascals
pounds (force) per square in.	6.894757	kilopascals
square ft	0.09290304	square meters
square in.	6.4516 E-04	square meters

List of Symbols

AA	Aluminum Alloy
AFCEC	Air Force Civil Engineer Center
AM2	Airfield Mat 2 (U. S. Navy design)
ASAALT	Assistant Secretary of the Army (Acquisition, Logistics, and Technology)
ASCE	American Society of Civil Engineers
ASTM	ASTM International
C	Number of applied coverages
C-17	Boeing C-17 Globemaster aircraft
C-130	Lockheed Martin C-130 Hercules aircraft
C-141	Lockheed C-141 Starlifter aircraft
C_c	Soil compression index
CBR	California Bearing Ratio (measure of soil strength)
D	Vertical displacement
D_{field}	Full-scale experiment vertical displacement
d_{lab}	Laboratory vertical displacement
δ_m	Plastic deformation of mat surface
δ_s	Plastic deformation of subgrade
E_c^{NJ}	Composite modulus of elasticity of mat system absent the joints
E_{flex}	Flexural modulus of elasticity
EI	Flexural rigidity
ε_p	Plastic strain
ERDC	U. S. Army Engineer Research and Development Center
F-4	McDonnell Douglas F-4 Phantom fighter jet
F-15E	McDonnell Douglas F-15E Strike Eagle fighter jet
FE	Finite element analysis
GSL	ERDC's Geotechnical and Structures Laboratory
I	Moment of inertia
I_{trans}	Moment of inertia for AM2 in the transverse loading direction
I_{long}	Moment of inertia for AM2 in the longitudinal loading direction
L	Longitudinal loading direction
L	Span between supports
N	Number of repeated load cycles
N_f	Number of allowable C-17 passes to system fatigue failure
$N_{f\text{-}1}$	Number of allowable F-15E passes to one panel failure

$N_{f\text{-}4}$	Number of allowable F-15E passes to system fatigue failure
$N_{f\text{-}lab}$	Number of allowable laboratory cycles to specimen fatigue failure
$N_{f\text{-}lab\text{-}avg}$	Average number of allowable laboratory cycles to specimen fatigue failure
P	Equivalent single wheel load
P_f	Applied force
P_n	Number of passes
PSP	Pierced Steel Plank airfield matting
R^2	Coefficient of variation
RCI	Rating Cone Index (soils)
S_c	Slope correction factor
σ_d	Deviator stress
σ_s	Soil static strength
t	Thickness
T	Transverse loading direction
W_{field}	Width of full-scale experiment subgrade deformation
w_{lab}	Width between laboratory loading and pivot constraints
WES	U.S. Army Waterways Experiment Station

1 Introduction

1.1 Introduction and background

When the first aircraft were invented in the early 1900s, they were lightweight and only required a relatively smooth grass or dirt surface to operate. As flight and mechanical knowledge increased, more sophisticated aircraft were developed that required a more substantial operating surface, such as a prepared air strip made from compacted gravel. In the 1930s, the world's militaries had begun to develop heavy aircraft for use as war machines that required paved surfaces to keep the aircraft from sinking into the soft unsurfaced areas typical of airfields of the time period. As aircraft were being massed in staging areas in Europe prior to World War II, there were only limited paved areas adjacent to the airstrips to park aircraft. Grass fields had to be used for additional parking. Because the large bomber aircraft were heavy and had relatively high tire pressures, they began to sink into the ground and become immobilized, causing concern from military leadership.

The British developed wooden mats that could be placed on the ground underneath the aircraft to distribute the wheel loads and keep the aircraft from sinking. When the U.S. military began to send war planes to Europe, they quickly realized a more substantial matting system was required to further expand parking areas for heavier aircraft. A steel matting system was developed in the early 1940s called Pierced Steel Plank, or PSP, that could be mass-produced by many steel mills in the United States, was easily transportable, was reusable, and offered a great improvement over the existing wooden mats in terms of its ability to distribute the aircraft loads over a large area of subgrade. The success of the PSP system for rapidly constructing stable operating surfaces led to production of over 900 million ft^2 from the 1940s through the 1960s.

Since the inception of PSP, many countries around the world, including France, Great Britain, the former Soviet Union, and the United States, have developed airfield matting systems using increasingly lighter and more modern materials in response to needs driven by changes in aircraft designs. Researchers have struggled to develop reliable methods to predict the subgrade and mat response under aircraft loading without conducting full-scale testing. Several full-scale test sections were constructed at the

U.S. Army Engineer Waterways Experiment Station (now the U.S. Army Engineer Research and Development Center [ERDC]), with California Bearing Ratios (CBRs) ranging from 4 to 10 percent, from the 1950s through the 1970s to develop equivalency curves for variants of airfield mats. The methods used to develop the equivalency curves equated the mat-surfaced area to an equivalent thickness of flexible pavement using the CBR design procedure for airfields. These equivalency curves were used for a limited number of airfield mat designs that were constructed from aluminum and steel.

The U.S. Navy designed the AM2 matting system from an aluminum extrusion in the late 1960s and it remains the primary system used by the U.S. military at present. Since the initial testing was performed on AM2 in the 1960s, several changes have occurred in regards to aircraft using AM2. Most notably, the original controlling design fighter aircraft, the F-4 Phantom, was replaced by the F-15E Strike Eagle and the controlling cargo aircraft, C-141 Starlifter, was replaced by the C-17 Globemaster. Significant differences in the tire pressures, gear configurations, and gross vehicle loads warranted new performance tests to determine if the original equivalency curves developed in the 1960s were still relevant. Furthermore, the minimum subgrade strength underneath a mat surface allowing for aircraft operation was increased from a CBR of 4 to 6 percent. These changes in loading and support strength led researchers to conduct new tests using the modern boundary conditions.

A series of full-scale experiments were designed, constructed, and executed by the ERDC's Airfields and Pavements Branch (APB) over different subgrade strengths and types to gather the data required for comparison. A total of nine full-scale traffic experiments were conducted from 2005 through 2013 on AM2 matting with funding provided by the U.S. Air Force. These experiments were performed in the Hangar 4 covered airfield pavement test facility on the ERDC Vicksburg, MS, campus and were accomplished by constructing highly controlled soil/subgrade test beds with CBRs of 6, 10, 15, 25, and 100 percent. The subgrades with CBRs of 6, 10, 15, and 25 percent were constructed using "Vicksburg Buckshot" high-plasticity clay and the CBR of 100 percent experiment was constructed using a standard 610 crushed limestone material. The prepared surfaces were covered with AM2 matting and trafficked with actual F-15E and C-17 aircraft main landing gears mounted on specially design trafficking vehicles. The amount of data collected from these experiments was enormous,

and its generation enabled the ability to improve upon existing equivalency curves for performance prediction.

The research presented in this report utilizes data collected from the nine full-scale traffic experiments on AM2 airfield matting to advance the state-of-knowledge for predicting AM2 airfield mat performance under modern aircraft loads for the entire spectrum of subgrade CBRs. The three primary objectives of this report are to:

1. Provide improved relationships to predict the deformation performance of the subgrade underneath an AM2 mat expanse based on the in-situ CBR for the F-15E and C-17 aircraft.
2. Provide relationships to predict fatigue damage, in terms of passes to failure, of an AM2 mat expanse based on the in-situ CBR of the underlying subgrade for the F-15E and C-17 aircraft.
3. Present a new laboratory approach to evaluate an AM2 style joint in fatigue that can be related to field performance and can predict cycles to failure without the expense of a full-scale test section.

The relationships developed by this research are envisioned for implementation into practice by the U.S. military to improve design and evaluation procedures for AM2 surfaced airfields to aid mission planners with better risk-reduction tools. The laboratory methods presented herein are being immediately implemented by researchers within the ERDC into new projects aimed at designing new lightweight matting systems by offering a tool representative of field boundary conditions to evaluate new airfield mat joint designs and materials.

1.2 Organization of study

The body of this report is a compilation of three complementary articles that describe different components of the main objectives and results from the full-scale experiments on AM2 mat-surfaced airfields. The report is organized into five chapters. The first chapter is the introduction and the last chapter, Chapter 5, is the conclusion and recommendations. The three chapters in the middle represent three manuscripts, in various stages of review or publication, which contribute to and support the three main objectives of this report outlined previously in this chapter. Chapter 2 presents the development of a subgrade deformation relationship for F-15E traffic over an AM2 mat installation. Chapter 3 presents a relationship of low-cycle fatigue damage behavior of AM2 and a novel

laboratory test fixture and procedure to predict fatigue damage under F-15E traffic. Chapter 4 presents the subgrade deformation and fatigue relationships for an AM2 installation subjected to C-17 aircraft loading and evaluates the validity of the laboratory test method presented in Chapter 3 for the F-15E for the complex loading of the C-17 aircraft.

At the time of the writing of this report, the article represented in Chapter 2 has been published as a peer-reviewed journal article in the Journal of Terramechanics, the article presented in Chapter 4 has been published as a peer-reviewed journal article in the ASCE Journal of Materials in Civil Engineering, and the article presented in Chapter 4 has been published as a peer-reviewed journal article in the ASTM International Journal of Testing and Evaluation. Some minor modifications have been performed to the as-submitted documents to meet the formatting requirements of this report; however, the technical content has not been altered. As applicable, permission has been obtained to reproduce the content in this document that is published in peer-reviewed journals.

2 Prediction of Soil Deformation Beneath Temporary Airfield Matting Systems Based on Full-Scale Testing

This chapter represents the final draft of an article that has been published by Elsevier as an article in Volume 58 of the *Journal of Terramechanics*. The as-published article can be accessed using the following internet address: http://dx.doi.org/10.1016/j.jterra.2014.12.004. The article (Rushing and Howard 2015) has been reformatted and reproduced herein with minor modifications to meet the formatting requirements of this report following the permission guidelines published by Elsevier.

2.1 Abstract

This paper presents results from full-scale evaluations of an aluminum structural mat system with regard to carrying heavy aircraft across graded, but unimproved, soil with California Bearing Ratios (CBRs) of 6, 10, 15, 25, and 100 percent. The objective was to determine relationships among soil deformation rate, the mat's flexural modulus, the number of applied passes, and the underlying soil's CBR. Current prevailing performance prediction models for aluminum mat systems are based on full-scale tests using historic aircraft loads over soils having a CBR of 4 percent that were never validated for soils with higher CBR values. Full-scale test results presented herein demonstrated the inability of current models to accurately predict mat permanent deformation. Strong correlations were found between measured and predicted data across the entire spectrum of soil CBRs. These relationships can be used to noticeably improve the accuracy of performance prediction models. An empirical equation was developed to reasonably predict subgrade deformation for any number of passes and soil CBR for the loading and mat system tested.

2.2 Introduction

Structural mat systems have been used to create temporary roads and aircraft operating surfaces for many years. Mat systems are typically individual structural panels that can be placed directly over soft soils and assembled in a continuous array using mechanical connectors to create vehicle operating surfaces. AM2 is an aluminum matting system that was designed by the U.S. Navy and is manufactured exclusively for the U.S. military. Figure 1 shows an example of bundles of AM2 aluminum

airfield mat panels, an AM2 cross-section extrusion, and an aircraft operating on an AM2 mat surface. Most steel and aluminum systems used in the United States were developed for military applications; however, composite systems are commercially available for use by the petroleum, construction, and event industries for reusable roads, work platforms, and turf protection (Rushing and Howard 2011).

Figure 1. AM2 aluminum airfield mat examples, (a) AM2 aluminum airfield mat panels prior to installation, (b) MV-22 aircraft operating on an AM2 mat surface, and (c) AM2 extrusion cross section.

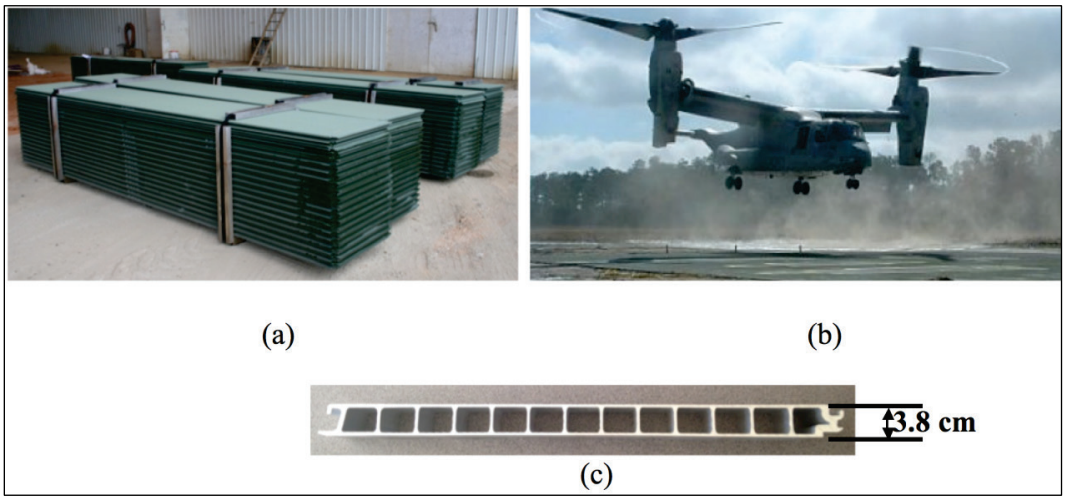

The ability to predict the number of allowable passes across matting systems, especially for aircraft, presents formidable challenges because of their complex designs, unique material compositions, and the difficulty predicting soil behavior under confined stress states. Previous and current prediction models known to the authors of this chapter's content were all based on full-scale test section data over soils with California Bearing Ratios (CBRs) ranging from 4 to 10 percent. Until recently, no full-scale data was available to validate prediction models over the full spectrum of soil-bearing capacities. Recently, testing has been conducted for CBRs of 6, 10, 15, 25, and 100 percent in an attempt to gather enough data to develop and validate new prediction models.

The objective of this paper is to determine the relationship for the rate of subgrade deformation, the number of applied passes, and the subgrade CBR from measurements obtained from full-scale traffic testing of mat-surfaced subgrades with CBRs of 6, 10, 15, 25, and 100 percent. The relationship described herein is specifically for AM2 matting systems, single-wheel gear military fighter aircraft traffic, and a normally

distributed traffic pattern. The overall research objective is to advance the ability to predict mat behavior under various types of aircraft traffic. Successful achievement of this goal stands to be useful to a wider segment of the terramechanics community than just the military (e.g., using the data presented herein for AM2 for benchmarking other rapid construction approaches or commercially available matting systems). The full data set is fairly comprehensive for AM2 matting under simulated military fighter and cargo aircraft loads. Companion work intends to evaluate damage to the mat itself caused by fatigue. Future work also intends to characterize rutting and mat damage behaviors for other aircraft loads and multiple wheel gear configurations. As discussed in the next section, previous work on matting has been predominantly focused on testing with a much smaller focus on analysis and prediction model development. Narrowly focused data sets have been used for analysis/prediction efforts in many cases.

2.3 Background

Since the 1940s, millions of U.S. dollars have been spent testing matting systems, with a considerable portion of these efforts performed at the U.S. Army Waterways Experiment Station site in Vicksburg, MS. While they are not cited for brevity, a casual search found over 70 reports on matting systems. The overwhelming majority of these reports were test reports, with only a few specifically addressing analysis, characterization, or prediction model development. The background presented herein focuses on the non-testing aspects of matting research, as this is the area of primary interest in this paper.

Throughout the four decades spanning the 1940s through 1970s, several steel and aluminum mat systems were tested using full-scale aircraft simulators. A review of ten test reports from aluminum systems revealed nearly all were conducted over a 60 cm (24 in.) deep soil test bed with a nominal CBR of 4 percent (White 1971a, 1972, 1973, 1974; Smith 1972; Green and McCormick 1971; Carr 1972, 1973, 1974; Green 1972). Applied loadings were 12 kN (27,000 lbf) on a single-wheel with a tire inflated to 2750 kPa (400 psi). Many of the tests were developmental or qualification experiments. Flexural properties of the mat systems were not documented.

Most past analysis has consisted of inputting data, representing a single failure point from one full-scale test, into Equation 1 to determine the equivalent thickness of flexible pavement provided the mat. The

equivalent thickness is based on typical airfield asphalt failure criteria of about 25 mm (1 in.) of rutting or reaching some crack development limit.

$$t = (0.23logC + 0.15)\sqrt{P\left(\frac{1}{8.1CBR} - \frac{1}{p\pi}\right)} \quad (1)$$

In Equation 1, t = total thickness (in.) of flexible pavement above the subgrade (for a standard airfield pavement design of asphalt over granular base), C = number of aircraft coverages (no units), P = single or equivalent single-wheel load (lbf), CBR = measure of subgrade strength, and p = tire contact pressure (lbf/in.^{2}). Equation 1 was derived from the CBR design equation (Ahlvin 1991) for flexible pavements in English units. The CBR design method is based on single-layer load/deflection theory with empirically derived factors from full-scale pavement test sections. The CBR method remains the predominant design procedure for flexible airfield pavements for the U.S. military.

Using inputs for C, P, CBR, and p from a full-scale mat test, an equivalent thickness of flexible pavement, t, was calculated using Equation 1 that provided the same load support for the loading and subgrade condition found in the full-scale tests. Once an equivalent thickness was determined, Equation 1 was solved for the number of allowable coverages, (C), for a given soil CBR, which was then translated to allowable passes based on the aircraft's pass-to-coverage ratio.

While this method offered a reasonable correlation for weaker soils (i.e., CBR <10 percent), damage progression is not necessarily linear and it can vary noticeably for asphalt and mat systems because of their grossly different material properties. The two materials should not be expected to follow the same nonlinear damage trends as a function of CBR. Using the equivalent thickness of asphalt pavement for a mat system greatly overpredicts the number of allowable passes for soils with CBRs greater than 10 percent; however, mat systems are often installed where the subgrade is much stronger. Even with its limitations, this approach is still the primary method used to predict mat performance.

Recent attempts to improve prediction methods have been made with some successes. In 2010, Gonzalez and Rushing (2010) used a finite element (FE) analysis back-calculation procedure described by Berney et al. (2006) to determine the unit section modulus, EI (or flexural rigidity) for

several different mat systems. Using the results and those from full-scale testing, Gonzalez and Rushing (2010) determined the maximum deviatory stress applied to the subgrade and used a stress-based approach to develop a mechanistic model to predict passes-to-failure based on subgrade CBR. The model was based on CBRs ranging from 6 to 15 percent and did not consider higher strength soils. While it offered some improvement, it did not attempt to characterize subgrade deformation rate nor mat breakage, in terms of fatigue, and it is not currently being used in practice.

Rushing and Howard (2011) presented full-scale data from 11 truck-loaded road mat systems. The deformation rate was predicted using the equation of the best fit logarithmic function through the measured deformation points for each system. The equations showed strong correlations to the measured data in terms of passes and deformation but were only applicable when the subgrade CBR, mat type, and applied load were similar to the testing conditions. Doyle et al. (2014) compared stress predictions using FE methods to those measured from earth pressure cells installed in full-scale test sections described by Gartrell et al. (2009). The authors found that FE showed potential for improving the ability to predict damage to the subgrade and mat system; however, more information from full-scale testing was required to further calibrate the model. Better flexural modulus information was also needed, especially around the mat joints to further refine the FE model.

Although some recent progress in mat performance predictability has been made, there still have not been many (if any) attempts to determine mat behavior over the full CBR range. Additionally, the systems investigated by Doyle et al. (2014) and Gartrell et al. (2009) were made of fiberglass and plastic and did not account for more rigid aluminum systems that are predominantly used by the U.S. military. The design procedure described by Gonzalez and Rushing (2010) was the most comprehensive approach of direct pertinence to this paper but failed to separate damage models such as subgrade deformation and mat fatigue failures. Researchers determined that full-scale tests were needed to validate prediction models on higher strength soils. Therefore, data were collected from 2006 through 2008 over soils with CBRs of 6, 10, and 15 percent (Rushing and Tingle 2007; Rushing et al. 2008; Rushing and Mason 2008). Tests were added to the initial series in 2012 over soils with CBRs of 25 and 100 percent (Garcia et al. 2014a; Garcia et al. 2014b). The information collected for these studies

was used herein to determine the rate of subgrade deformation for the five subgrade strengths.

2.4 Full-scale test sections

Five full-scale test sections having subgrade CBRs of 6, 10, 15, 25, and 100 percent were constructed and trafficked to obtain the deformation data presented in this paper. Test sections were constructed in a covered test facility so test section moisture, and therefore bearing capacity, would remain relatively constant (with the exception of densification and/or damage during trafficking). Each of the full-scale experiments consisted of a plastic-lined 60 to 90 cm (24 to 36 in.) deep subgrade constructed in 15-cm (6-in.) lifts. Each lift was subjected to field CBR measurements in accordance with U.S. Army Corps of Engineers (1995) Standard CRD-C 654-95 to ensure the required CBR was reasonably achieved. If the CBR of a lift varied more than ±0.5 percent CBR from the required value, the lift was removed from the test section, reprocessed, and replaced until the CBR was within the required range. Each test section was 7.3 m (24 ft) wide and 12.2 m (40 ft) long and was surfaced by placing a structural mat system directly on top of the prepared soil.

Traffic was applied using an aircraft simulator (Figure 2) with a single-wheel loading of 157 kN (35,235 lbf) on a tire inflated to an internal pressure of 2,240 kPa (325 psi). The net contact area of the tire was approximately 706 cm² (109.5 in.²) and determined from the digitization of a painted imprint. Traffic was applied over five traffic lanes that were 23 cm (9 in.) wide, for a total traffic width of 115 cm (45 in.). The two outer lanes received 50 percent of the traffic applied to each of the three center

Figure 2. Aircraft simulator (a) Overall view of test section and (b) Close-up view of load wheel.

lanes to create a relatively normal traffic distribution that was simplified for ease of use by the test vehicle operator.

The term *coverage* as used in this paper is defined as the number of times the test wheel crosses a single point in the center traffic lane of the test section. A *pass* is defined as a single crossing of the test section by the test vehicle (either forwards or backwards). The *pass*-to-*coverage* ratio is the inverse of the sum of probabilities that the aircraft tire will cross a given point on the pavement during a *pass*. A *pass* and a *coverage* are one and the same when the test wheel is in the center traffic lane. Using this paper's data collection as one example, traffic was applied by driving the test vehicle forward and then backward across the test area in an outer lane and then shifting laterally 23 cm (9 in.) on each forward *pass* to the adjacent lane. After a total of 16 passes, the outer lanes had received 2 passes, and the 3 interior lanes (including the center lane) had each received 4 passes. The *pass* to *coverage* ratio for the center traffic lane was determined by dividing 16 total passes by 4 crossings of the center traffic lane. Therefore, the *pass* to *coverage* ratio for this test was 4.0. The traffic pattern was continued until the measured subgrade deformation exceeded a minimum of 3.18 cm (1.25 in.) or the mat system could no longer support additional traffic because of structural failures caused by low-cycle fatigue of critical system components. Structural failure was determined from visual inspections of the mat surface. Failure was defined as any damage that presented a hazardous condition to the aircraft tire (i.e., sharp edges or protruding components) or caused instability in the simulator because of loss of structural support. All five test sections discussed in this paper were trafficked until structural failure was achieved.

2.5 AM2 mat system flexural properties

AM2 matting is created from a single 6061-T6 aluminum extrusion (Figure 1c). Each panel measures 61 cm (2 ft) wide by 366 cm (12 ft) long and is connected to adjacent panels using mechanical connectors. The test panels were newly manufactured with no previous fatigue history. The panels were assembled in a brickwork pattern and oriented so the 366-cm- (12-ft-) dimension was perpendicular to the traffic direction; i.e., 366-cm dimension was in the longitudinal (L) direction (Figure 2a).

Flexural properties of AM2 were determined by a 3-point bending test using a universal testing machine where load and vertical displacement were measured. Three replicates were performed for both the transverse

(T) and longitudinal (L) orientations (Figure 3). The T direction is described as the strong bending axis along the 61-cm- (2-ft-) panel dimension and parallel with traffic, and the L direction is described as the weak bending axis along the 366-cm- (12-ft-) panel dimension and perpendicular to traffic. The test was displacement controlled at a loading rate of 2.5 mm/min (0.1 in./min). Each test specimen measured 3.8 cm (1.5 in.) thick by 16.5 cm (6.5 in.) wide by 61 cm (24 in.) long. Specimen width was chosen to attempt to ensure the global bending properties of the system were approximated while staying within the capability of the test machine. The support span for the test was 45.4 cm (17.9 in.).

Figure 3. Load-displacement results for 3-point bend tests and photos of test directions. Joint behaviors were not considered in either direction.

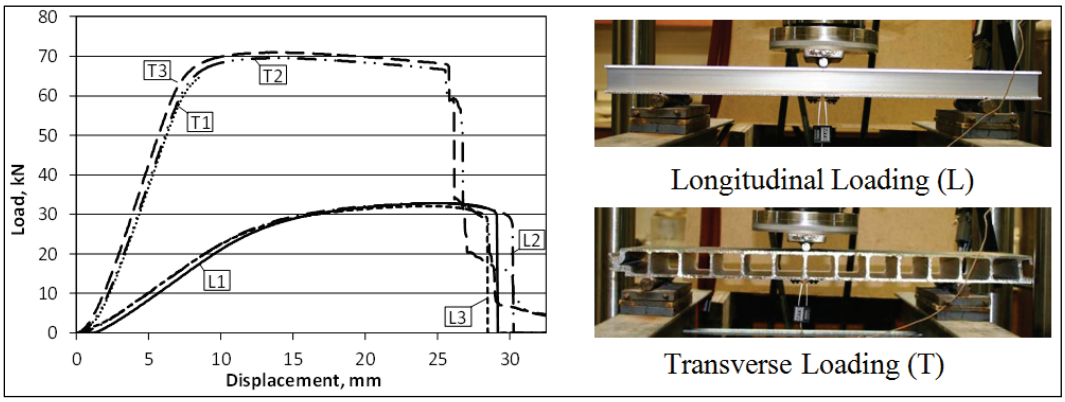

The area moments of inertia based on cross-section geometry were calculated as I_{trans} = 4.81 × 10^5 mm^4 (1.156 in.^{4}) and I_{long} = 4.47 × 10^5 mm^4 (1.075 in.^{4}). Test results are shown by replicate in Figure 3. The flexural modulus, E_{flex} (MPa), values shown in Table 1 were determined from Equation 2,

$$E_{flex} = \frac{L^3 P_f}{48ID} \quad (2)$$

where L is the span between supports with units of mm (in.), P_f is the applied force with units of N (lbf), I is the sample moment of inertia in mm^4 (in.^{4}), and D is the displacement resulting from the force with units of mm (in.).

Force-displacement pairs, P1-D1 and P2-D2 (shown in Table 1), were chosen as two points along the linear elastic portion of the load versus displacement curves shown in Figure 3. During test T1, a limit was tripped on

the testing device, causing the test to complete prior to reaching the yield point as shown in Figure 3.

Table 1. Flexural properties of aluminum mat tested.

Transverse Direction							
	P1, kN (kips)	P2, kN (kips)	D1, mm (in.)	D2, mm (in.)	ΔP/ΔD, kN/mm (kips/in.)	P_{max}, Kn (kips)	E_{flex}, 1 x 10^4 MPa (1 × 10^6 psi)
T1	44.48 (10.00)	17.93 (4.03)	5.8 (0.23)	3.0 (0.12)	9.48 (59.33)	NA	4.21 (6.10)
T2	44.70 (10.05)	18.19 (4.09)	5.6 (0.22)	3.0 (0.12)	101.96 (59.88)	69.53 (15.63)	4.25 (6.16)
T3	44.57 (10.02)	18.02 (4.05)	5.1 (0.20)	2.8 (0.11)	11.54 (62.33)	70.95 (15.95)	4.42 (6.41)
Average						70.24 (15.79)	4.30 (6.23)
Longitudinal Direction							
L1	17.84 (4.01)		8.6 (0.34)	5.3 (0.21)	2.70 (14.81)	32.87 (7.39)	1.13 (1.64)
L2	17.79 (4.00)	8.94 (2.01)	7.9 (0.31)	5.6 (0.18)	2.68 (14.79)	32.83 (7.38)	1.13 (1.64)
L3	17.84 (4.01)	8.94 (2.01)	7.9 (0.31)	5.6 (0.18)	3.87 (14.63)	32.07 (7.21)	1.12 (1.62)
Average						32.61 (7.33)	1.12 (1.63)

The flexural modulus was determined for the matting system to compare the stiffness and load distribution abilities with the rate of deformation measured in the test subgrade during trafficking. Knowing the relationship between structural mat system flexural modulus and subgrade deformation assists in behavior prediction of existing and future mat designs. For example, if a new system is required to meet or exceed the deformations measured for the aluminum system described, it is likely the flexural modulus must also be matched or exceeded. Systems with lower E_{flex} values should be expected to allow subgrade deformation to occur at a faster rate. The next section describes measured deformations as a result of full-scale testing.

2.6 Deformation measurements

Plastic deformation of the mat surface, δ_m, and plastic deformation of the subgrade, δ_s, was monitored at specified data collection intervals during trafficking so the rate of deformation could be compared for different subgrade strengths. The intent to test all five CBR conditions was not formed

until after the 6, 10, and 15 percent CBR test sections were completed; therefore, the data collection intervals and collection methods were somewhat varied between the tests. Even with the variability, enough data were collected to make a direct comparison.

Elevation data were collected by rod and level or total station along transverse data collection lines located at 3, 6, and 9 m (10, 20, and 30 ft) along the length of each test section. δ_s was difficult to monitor since the mat system was elastic and there were no holes in the mat surface to facilitate physical measurements. Measurements were attempted by recording elevation data on the unloaded mat surface and at the same location immediately adjacent to the load wheel of the test vehicle. The difference between the two measurements was the total elastic deflection of the mat and the subgrade underneath. The magnitude of the subgrade elasticity was unknown, using the described measurement procedure, and the elevation at 0.3-m (1-ft) intervals along quarter point location could not be measured with the test vehicle parked on the mat surface (since the structure of the test vehicle physically blocked measurement locations).

Another attempt was made to monitor δ_s by parking a 26.7-kN (6,000-lbf) forklift carrying 17.79 kN (4,000 lbf) of lead blocks immediately parallel to the transverse data collection lines. Elevation data was recorded at 0.3-m (1-ft) intervals for 3 m (10 ft) on each side of the traffic centerlines. The idea was to deform the mat panels enough to contact the subgrade surface without causing an elastic deformation of the subgrade. Data measured using this loaded deflection procedure was used to approximate δ_s. For the purposes of the analysis presented herein, δ_s is synonymous with the loaded deflection measurements.

Figures 4a and 4b show the deformation rates for δ_m and δ_s (loaded deflection measured on the mat surface), respectively, for the five subgrade strengths tested. The data were reported on a $\log_{10}$ scale to increase the resolution of the initial deformation and to show a somewhat linear progression, especially for δ_s as shown in Figure 4b. Initial zero pass values were changed to 0.1 pass so they could be reported on a logarithmic scale.

Figure 4. Rate of δ_m and δ_s for five subgrade CBRs (a) Rate of δ_m for five subgrade CBRs and (b) Rate of δ_s for five subgrade CBRs.

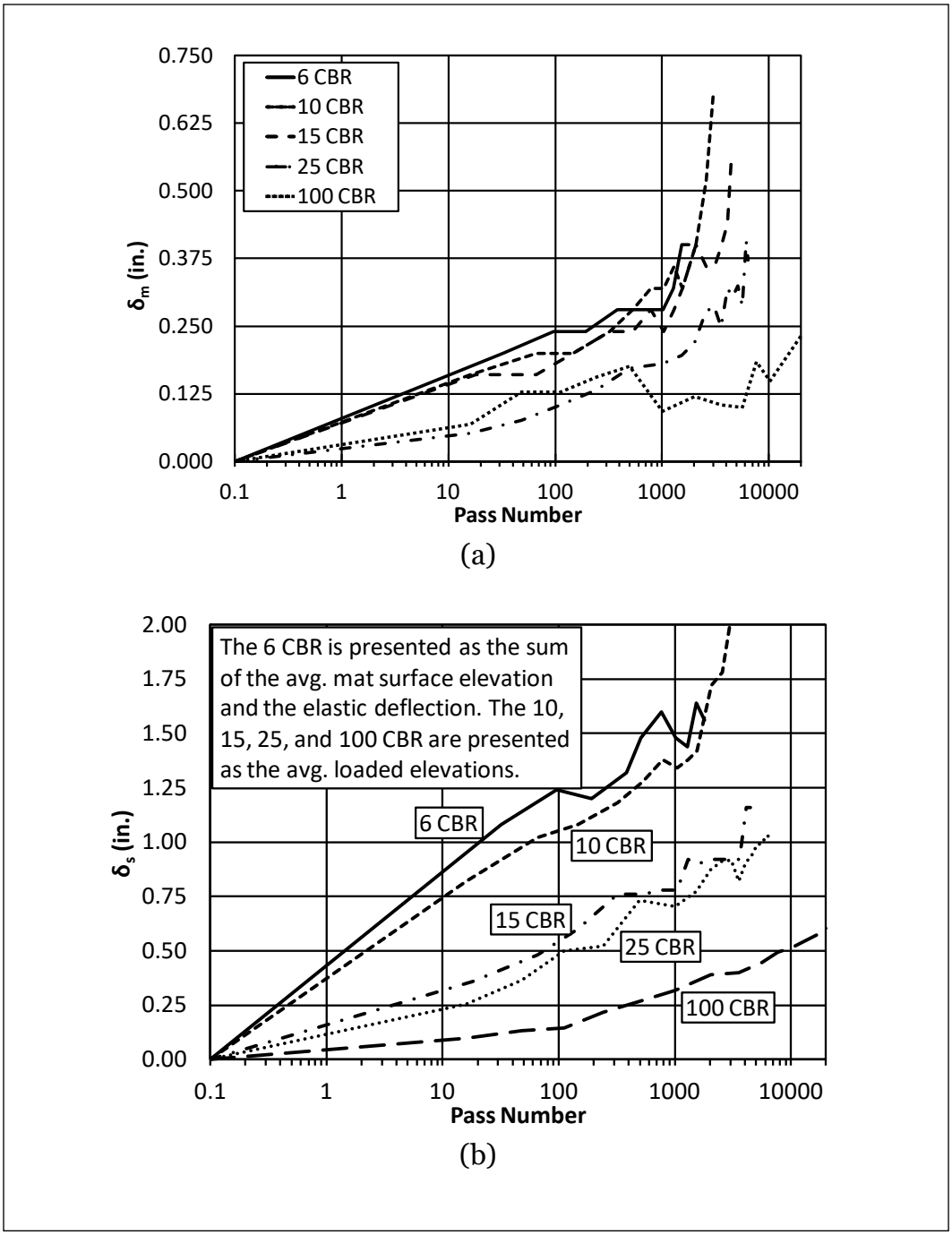

2.7 Analysis

Comparisons of δ_m and δ_s in Figures 4a and 4b indicate that a gap formed between the bottom of the mat and the soil surface since the rate of δ_s was

greater than δ_m for the relatively elastic mat. Also, δ_s and δ_m are inversely proportional to CBR since the rates of δ_s and δ_m decreased as the CBR of the subgrade increased, as shown in Figures 4a and 4b. The relatively linear trends of δ_s with respect to increasing numbers of passes shown in Figure 4b indicate that rut formation is inherently a logarithmic function, where the deformation increases quickly during the initial passes and then the rate of increase slows considerably.

Since all five test sections were trafficked until structural failure of the mat occurred, upward inflections in the deformation data shown in Figure 4b toward the end of the tests are most likely the result of yielding and breaking of the mat system. Once structural failures began to occur, the mat began to yield. Damage propagation caused the structure to weaken (lose its flexural modulus), and it could no longer support the test vehicle loads. Additional stress was transferred to the subgrade directly underneath the mat and resulted in an increase in the rate of deformation.

In an attempt to remove some of these biases based on structural mat failures, the data were revisited and analyzed according to the first 1,500 passes. The 1,500-pass cut-off point was chosen to match the minimum number of required passes for the structural mat system evaluated and to approximate the point of upward inflection for the 6, 10, and 15 percent CBR test results.

Logarithmic trend lines were fit to each data set to determine their ability to serve as predictors of permanent deformation (Figure 5a). The coefficients of determination, R^2, indicate a good predictability of the δ_s for all five associated subgrade strengths with respect to the number of passes from the full-scale test measurements.

The five logarithmic trend lines were forced through the origin by taking the $\log_{10}$ of the pass number and associating a linear trend line through the measured data points as shown in Figure 5b in an attempt to simplify the prediction model. For example, $\log_{10}$ of 1,500 is 3.17; therefore, the 1,500th pass was 3.17 units from the origin in the x-direction. The results showed that the R^2 values remained greater than 0.9 for all five CBR values, thus indicating strong prediction reliabilities while removing the y-intercept values from their respective equation. The difference in the rate of δ_s for each CBR was then related by the slope of the line when the $\log_{10}$ of the pass number was plotted.

Figure 5. δ_s Predictions using the first 1,500 passes (a) δ_s Predictions using the first 1,500 passes and (b) δ_s Predictions using the first 1,500 passes with origin forced through zero.

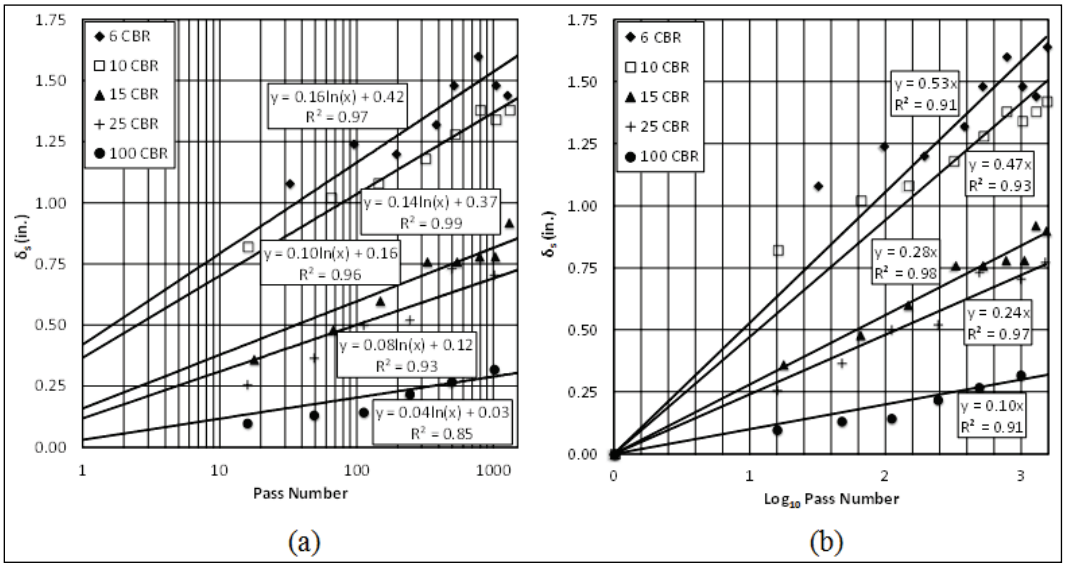

After the logarithmic functions relating passes to δ_s were determined, the next step was to see how δ_s was related to any given CBR and number of passes. δ_s was calculated for 10, 50, 100, 500, 1,000, and 5,000 passes for each of the five soil conditions tested using the prediction equations from the trend lines shown in Figure 5b. Data points for each pass interval were plotted with CBR on a $\log_{10}$ scale along the x-axis and δ_s on the y-axis. Power trends showed a strong relationship between CBR and δ_s for a given number of passes, with R^2 values of 0.98 for all five trends (Figure 6).

From Figure 6, δ_s based on CBR are related by a power function. Small CBR increases on the weak end of the spectrum cause large decreases in δ_s. As the CBR increases, the same increase in subgrade strength only allows minimal decreases in δ_s. Since the prediction equations in Figures 5b and 6 were simplified by forcing the trends through the origin, a simplified expression can be derived to solve for δ_s in terms of the number of passes and subgrade CBR (Equation 3), where δ_s = the subgrade deformation, in., P_n = the number of passes, and *CBR* is the CBR of the subgrade underneath the structural mat system.

Figure 6. Subgrade deformation predictions for a given number of passes and CBR.

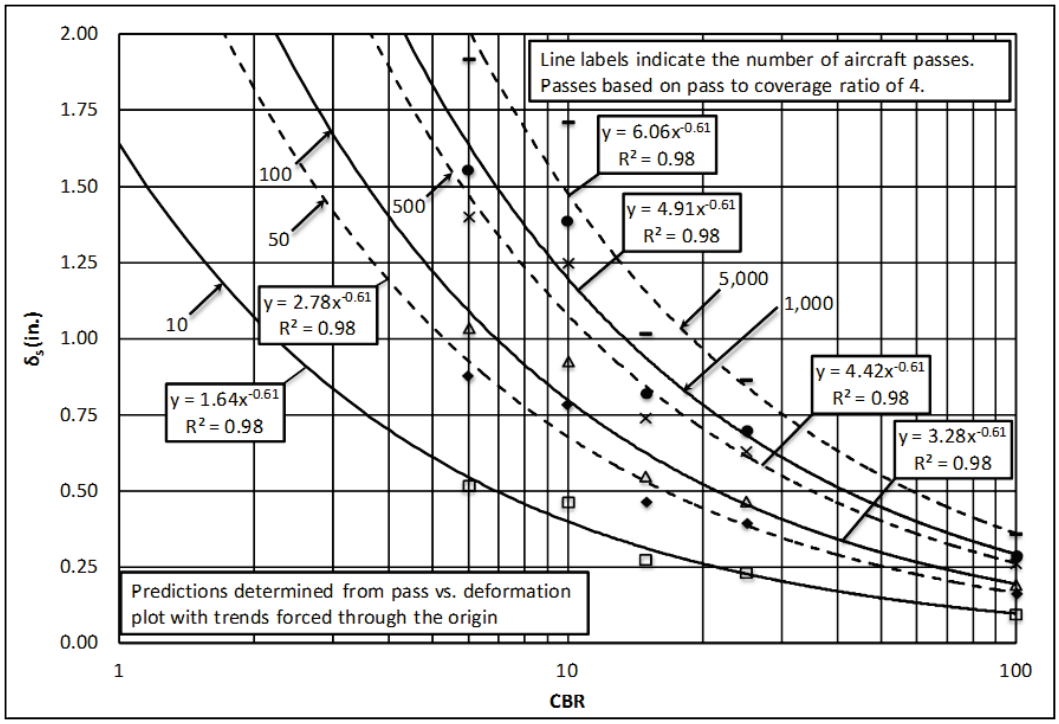

$$\delta_s = log_{10}P_n \cdot 1.64 \cdot CBR^{-0.61} \quad (3)$$

Equation 3 was used to develop a set of design curves (Figure 7) so a user can quickly read an approximate answer from the chart or use Equation 3.

For example, if 800 passes of fighter aircraft traffic was desired on an AM2 mat surface placed over a soil with a CBR of 8 before δ_s > 2.5 cm (1.0 in.), 800 would be entered for P_n and 8 for CBR is inserted into Equation 3 to solve for δ_s. The solution finds that δ_s is predicted to be 3.35 cm (1.32 in.). Therefore, a soil with a CBR of 8 percent would not be able to support 800 passes without exceeding a δ_s limit of 2.5 cm (1.0 in.). Additional strengthening of the subgrade or a reduction in the number of passes would be necessary to meet the requirements.

2.8 Prediction model comparisons

As discussed previously, the CBR design method is currently used to predict mat performance but is only reliable for soils with CBRs less than 10 percent. To demonstrate the significance of the prediction incompatibilities over higher strength subgrades using the CBR design procedure, data from full-scale tests of AM2 over subgrades with CBRs of 6 and

Figure 7. Subgrade deformation design curves.

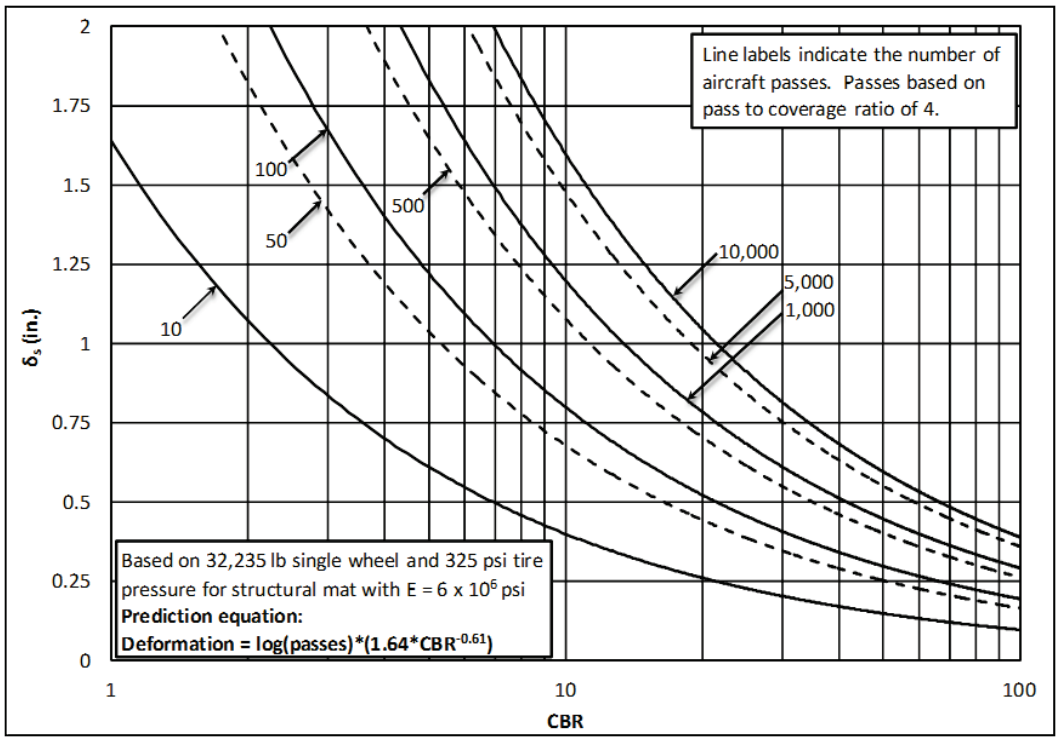

10 percent were investigated in terms of δ_s failures. Variables for the 6 percent CBR test in terms of Equation 1 were determined as C = 96, P = 35,235 lbf (156.7 kN), CBR = 6, p = 325 psi (2240.8 kPa), and *pass*-to-*coverage* ratio = 4.0. An equivalent flexible pavement thickness, t, of 15.9 in. (40.4 mm) was calculated. The equation was rewritten and solved for coverages, C, using t = 15.9 in. (40.4 mm) and CBR = 10 percent with all other variables held constant.

The solution to Equation 1 predicted 2,562 passes could be applied prior to δ_s failure if AM2 was placed on a 10 percent CBR subgrade; however, test results showed only 786 passes were actually achieved. For comparison, Equation 3 was solved for P_n using δ_s = 1.25 in. (3.18 cm) and CBR = 10 percent. The solution to Equation 3 predicted 1,274 passes, which was much closer to the measured result. Since AM2 is typically used for aircraft operations, predicting over three times the number of allowable operations is problematic. Table 2 gives a comparison of results for *CBR*s of 10, 15, 25, and 100 percent with δ_s = 1.25 in. (3.18 cm).

Table 2. Number of passes to δ_s failure vs *CBR* for measured and predicted conditions

CBR	Test Results	Equation 1	Equation 3	Equation 1 – Equation 3
6	384	NA	188	NA
10	786	2,562	1,274	1,288
15	> 4,482*	19,067	9,469	9,598
25	> 6,386*	646,400	269,229	377,171
100	> 23,000*	1×10^{23}	4×10^{10}	1×10^{23}

* Failed by mat breakage. Deformation limit was not reached.

2.9 Discussion of results

Equation 3 represents a more reasonable approximation of δ_s measured during full-scale tests on AM2 when subjected to fighter aircraft loading; however, there are two ways a structural mat system may fail during trafficking: (1) exceeding soil deformation limits and (2) breaking, or destruction, of the mat panels. Equation 3 is only used to predict δ_s. Further analysis is required to take the predicted δ_s and develop a step function to predict low-cycle fatigue-induced mat breakage to capture the second failure component.

The magnitude of strain in the mechanical joints of a mat system is at least partially a function of the vertical movement in the mat under an applied load. The δ_s for a given soil condition and the number of passes can theoretically be used to approximate the vertical displacement of the mat at any time (in terms of number of passes) during its life. Referencing the rutting model presented in this paper, a laboratory procedure could be developed using a step-amplitude function to test mat joint specimens to measure their fatigue life. A finite element model (e.g., approach by Doyle et al. 2014) could enhance determination of the critical location and magnitude of limiting stresses/strains and improve effectiveness of the investigation.

From the test section data, the mode of failure appears to transition from δ_s to mat breakage between CBRs of 15 to 25 percent. An overall prediction of mat performance will require both models before the entire spectrum of CBRs can be properly represented. Furthermore, functions need to be developed to enable prediction for an applied stress and mat system E_{flex}, similar to the approach described by Gonzalez and Rushing (2010) but

with refinement to include more representative flexural properties of the matting system being evaluated. Even though additional analysis is required, the ability to predict δ_s across the entire spectrum of subgrade strengths using full-scale test data is advancement toward the development of a global prediction model that should advance the state of the art in structural mat system design, evaluation, and use.

2.10 Summary and conclusions

The current model used to predict the number of allowable vehicle passes over structural mat systems placed directly over semi-prepared soils is based on flexible pavement design. This model greatly overestimates the number of allowable passes for soils with CBRs greater than 10 percent. The actual rates of δ_s for soils with CBRs of 6, 10, 15, 25, and 100 percent were determined through full-scale test sections. Analysis revealed that δ_s with respect to passes for a given CBR could be closely approximated using logarithmic trends. The relationship between the five logarithmic functions associated with soil CBRs were then approximated using power functions. A simplified equation was developed to enable a user to predict δ_s for any number of passes and soil CBR for the loading condition and AM2 structural mat system described in this paper. The empirically derived equation appeared to be a reasonable predictor of δ_s for the structural mat system and applied load tested in this paper.

2.11 Future work

Future work is planned to determine relationships of applied stress and mat system flexural modulus to the rate of subgrade deformation, δ_s. A model to improve the ability to predict δ_s for any mat system and applied loading may be developed once these relationships are known. Additionally, the δ_s rates presented herein are planned for use in developing stress amplitude models to determine the low-cycle fatigue performance of the structural components of a mat system. A more advanced model that considers both failure modes is envisioned for future development. Data sets for full-scale traffic testing of refurbished AM2 mats with pre-induced fatigue in critical components and alternate assembly patterns are available. These data sets may also be used to develop performance reduction factors based on realistic operational environments.

2.12 Acknowledgments

The full-scale experiments and resulting data presented in this chapter were obtained from research conducted at the U.S. Army ERDC, Geotechnical Laboratory, Airfields and Pavements Branch with funds provided by the U.S. Air Force Civil Engineer Center (AFCEC). The sponsor determined the scope of the study but did not assist in data collection, analysis, or writing. The support of AFCEC and ERDC personnel is gratefully acknowledged. Permission to publish this work was granted by the Director, Geotechnical and Structures Laboratory, U.S. Army ERDC.

3 Laboratory Characterization of Fatigue Performance of AM2 Aluminum Airfield Matting

This chapter represents the final draft of an article that has been published by ASCE in the *Journal of Materials in Civil Engineering*. The as-published article can be accessed using the following internet address: http://dx.doi.org/10.1061/(ASCE)MT.1943-5533.0001620. The draft article (Rushing et al. 2016) has been reformatted and reproduced herein with minor modifications to meet the formatting requirements of this report following the permission guidelines published by ASCE.

3.1 Abstract

AM2, an airfield matting system made from extruded 6061-T6 aluminum alloy, is used to construct temporary aircraft operating surfaces. This matting system can support heavy aircraft loads even when placed directly over graded in situ soils. This paper presents the development of a test protocol and corresponding relationships that can be used to predict fatigue failure of AM2's mechanical joints over any subgrade California bearing ratio (CBR) when subjected to high tire pressure single-wheel aircraft loading. First, full-scale simulated aircraft traffic experiments were conducted over sections of AM2 installed on subgrades with CBRs of 6, 10, 15, 25, and 100 percent to monitor subgrade deformation and fatigue failure. An increasing amplitude displacement function developed from a subgrade deformation model was then used to create a new laboratory procedure to simulate fatigue experienced by the matting system's complex mechanical connectors under moving aircraft loads. Laboratory test results had strong correlations with field data and, therefore, have promise for predicting fatigue performance without the expense of full-scale experiments.

3.2 Introduction and background

Airfield matting has been used by the U.S. military to create temporary operating surfaces for aircraft since the 1940s. AM2, the most commonly used airfield matting system, was designed by the U.S. Navy in the 1960s to support both fighter and cargo aircraft over graded yet unimproved soils for the creation of expeditionary airfields. Modern mat systems are typically individual interlocking planks made from various materials and are connected using complex mechanical joints and fastening systems.

Once assembled in an array, predicting mat performance in terms of allowable passes when subjected to aircraft loads becomes complicated. Predicting subgrade deformation underneath the mats and the physical damage to critical joint components further complicates the problem. Additional background on matting systems and their applications is provided by Rushing and Howard (2011, 2015).

As described by Rushing and Howard (2015), significant research was performed on airfield mat system designs by the U.S. Army Waterways Experiment Station (WES) from the 1940s through 1970s. Since the beginnings of airfield mat development and evaluation by the U.S. Army, at least 28 unique joint systems have been designed. To prevent panel movement and to allow for shear and sometimes moment transfer across the joints, 11 different locking mechanisms have been employed. The large number of joint types and the variability in the way they function have led to researchers largely ignoring joints from consideration in previous attempts to characterize the behavior of airfield mat systems.

Initial work describing the behavior of landing mats under aircraft loads evolved from considering matting systems as thin membranes of infinite extent and subgrades incapable of supporting shear stresses (Pickett 1951, 1955), to back calculating joint efficiencies for more advanced analysis (Harr and Rosner 1969), to acknowledging that even the most sophisticated models were unable to truly characterize matting performance and advances in computing were likely required to make more accurate performance predictions (White 1971b). Modern attempts to characterize airfield mat performance have still yet to fully characterize subgrade deformation and joint fatigue performance simultaneously.

Gartrell (2007) conducted a full-scale investigation on instrumented airfield mats and used two different two-dimensional rigid pavement models to compare field-measured and model-predicted subgrade stresses. Attempts to account for the joints were made by varying the load transfer percentages for shear and moment between adjacent slabs. Gartrell (2007) pointed out that a three-dimensional finite element approach was more suitable if detailed joint response was required. Neither model was able to account for accumulated damage nor approximate rutting in the subgrade caused by repeated or dynamic loads and did not consider mat fatigue.

Gartrell et al. (2009) evaluated five unique composite matting systems in full-scale test sections under simulated C-130 and C-17 aircraft loads. The authors presented detailed results of the evaluations but did not develop predictions for system performance. Gonzalez and Rushing (2010) used full-scale test section data and back-calculated modulus of elasticity values for matting systems to develop a mechanistic-empirical model using layered elastic theory. Their approach related maximum subgrade deviator stress, subgrade CBR, and coverages of aircraft traffic to failure of the systems. This approach also neglected the effects of mat system joints.

Doyle et al. (2014) investigated the matting systems studied by Gartrell (2007) using a three-dimensional finite element model to improve performance predictions. This approach used four-point bending data to differentiate the modulus values of the interior portion of the mat panel and the modulus of the longitudinal and transverse joints. Depending on the joint type (i.e., overlap/underlap, hinge, bolted, etc.) the stresses transmitted to the subgrade caused by an applied load placed above the joint may increase or decrease as compared to loads applied in the center of the mat panel. Results of the analyses correctly identified the areas of maximum stress. The model developed by Doyle et al. (2014) was able to approximate the measured stresses underneath the matting systems and could be used as a preliminary mat selection tool. However, the authors concluded that further research is needed to develop transfer functions to predict rut accumulation and joint damage.

Although some recent progress in mat performance predictability has been made, there have not been any attempts, to the authors' knowledge, to determine the fatigue performance of the mat joints, especially as related to accumulating subgrade deformation. However, fatigue is one of the most critical failure mechanisms of a matting system, and the relationship of fatigue to subgrade deformation is important to predict the number of allowable load cycles that will cause system failure. The following paragraph summarizes works of potential relevance dealing with aluminum fatigue that emphasize the gap in literature this paper attempts to address.

Zwerneman and Frank (1988) investigated the effect of variable amplitude loads on compact-type steel specimens to estimate the fatigue crack growth in in-service bridges. Azzam and Menzemer (2006) evaluated welded aluminum light pole support details using full-scale constant amplitude fatigue experiments to determine the fatigue life to compare

with design provisions. Saleem et al. (2012) evaluated extruded aluminum bridge deck components under high-cycle constant amplitude experiments to determine the feasibility of use for lightweight highway bridge decks. Coughlin and Walbridge (2012) investigated the high-cycle fatigue resistance of aluminum welds under in-service highway bridge loading conditions using constant stress amplitudes. These four studies address fatigue behavior of transportation structures, but none of them use an increasing amplitude function that can be related to subgrade deformation underneath a structure and are not applicable to the fatigue behavior of mat joints.

3.3 Objectives and scope

The objective of this paper was to develop a model to predict the low cycle fatigue damage in an AM2 airfield mat system for a single-wheel loading for any given subgrade condition. The subgrade deformation model developed by Rushing and Howard (2015) was used to create an increasing amplitude laboratory procedure to simulate subgrade deformation in displacement controlled fatigue experiments. This new method was able to predict joint failures without the expense of constructing full-scale test sections and conducting simulated aircraft trafficking tests. This paper describes: (1) the development of an equation to predict fatigue failure in AM2 matting under single-wheel aircraft loading, (2) the methods used to create the laboratory fatigue experiments, (3) the results of the fatigue experiments, and (4) the validation of the lab data with respect to full-scale test results. To the best of the knowledge of the authors of this chapter's content, the work presented in this paper was the first attempt at laboratory characterization of the fatigue performance of the AM2 matting system (or similar matting systems) under single-wheel aircraft loading.

The scope of this effort includes (1) a series of five full-scale simulated aircraft traffic tests conducted on controlled testbeds surfaced with AM2 matting with CBRs of 6, 10, 15, 25, and 100 percent and (2) displacement controlled laboratory experiments developed using data collected from the full-scale experiments.

3.4 Material properties

The current version of AM2 is Mod-5 and is comprised of 6061-T6 aluminum alloy (AA6061-T6) extruded into 366-cm- (12-ft-) long by 61-cm- (2-ft-) wide by 3.8-cm- (1.5-in.-) thick full panels and

183-cm- (6-ft-) long by 61-cm- (2-ft-) wide by 3.8-cm- (1.5-in.-) thick half panels (Figures 8a and 8b). The system consists of male/female hinge type connections along the length of the panels with overlap/underlap mechanical connections applied by fusion welding along the 61-cm (2-ft) ends. Figures 8c and 8d are photos of AM2 style joints to show the complexity of the system and the joint concept only; however, close-up photos of the actual AM2 joints are not shown because the details of the joint are not publicly available. After adjacent overlap/underlap joints are assembled, a solid rectangular shaped AA6061 locking bar is inserted into a formed slot in the connection to prevent vertical separation of the panels along the joint.

Figure 8. AM2 installation and joint assembly (a) AM2 matting panel being installed in a controlled full-scale test section, (b) Locking bar being inserted between adjacent panels to prevent vertical separation of joints, (c) AM2 style (i.e., not AM2) male/female hinge joint, and (d) AM2 style (i.e., not AM2) overlap/underlap joint.

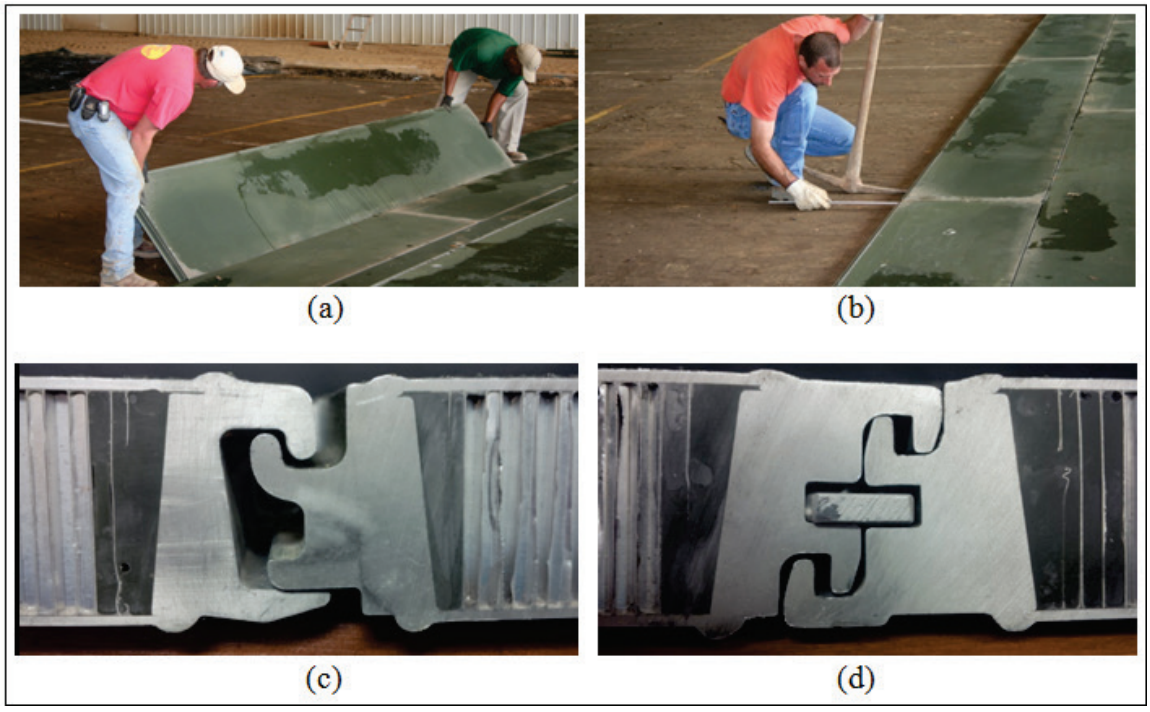

Because 6xxx series alloys (AA6061 is an example) are among the easiest to extrude, they are ideal for complex parts such as AM2's hollow core extrusion. AA6061 is a good compromise between strength and extrudability. Table 3 presents the mechanical properties of the extruded AA6061 in the T6 condition, where the T6 is a precipitate hardening heat treatment for AA6061. The nominal chemical composition of AA6061 is given in Table 4.

Table 3. AA6061-T6 mechanical properties.

Tensile Ult. Strength, MPa (ksi)	Tensile Yield Strength, MPa (ksi)	Tensile Elongation	Barcol Hardness	Compress Modulus, GPa (Msi)	Compress Yield, MPa (ksi)
303 (44)	283 (41)	11%	80	71 (10.3)	300 (43.5)

(Data from Allison et al. 2014).

Table 4. Chemical composition of AA6061 (weight percent).

Element	Mg	Si	Cu	Mn	Fe	Cr	Al
Min.	0.8	0.4	0.15	-	-	0.04	Bal.
Max	1.2	0.8	0.4	0.15	0.01	0.35	Bal.

(Data from Jogi et al. 2008).
Bal. means all remaining components are Al.

3.5 Full-scale experiments

Full-scale experiments consisted of constructing 91-cm- (3-ft-) deep test beds of soil inside a covered pavement test facility. The foundation for each test bed was lined with plastic to prevent moisture migration into or out of the test bed. The majority of the test beds were approximately 21.3 m (70 ft) wide by 12.2 m (40 ft) long. The foundation soil was processed to the desired moisture content and placed and compacted in 15-cm (6-in.) lifts to achieve the desired test CBR. Details of the full-scale tests over CBRs of 6, 10, 15, 25, and 100 percent are described in U.S. Army Engineer Research and Development Center (ERDC) Technical Reports (Rushing and Tingle 2007; Rushing et al. 2008; Rushing and Mason 2008; Garcia et al. 2014a, 2014b). In-situ CBR tests were conducted in accordance with U.S. Army Corps of Engineers (1995) *Handbook for Concrete and Cement: Standard Test Method for Determining the California Bearing Ratio of Soils* to ensure the desired strength of each lift had been reasonably achieved.

Once the soil test bed had been constructed, the AM2 matting system was assembled in a brickwork pattern as shown in Figure 8a and then trafficked using a single-wheel aircraft simulator as shown in Figure 9. Traffic was applied using a normally distributed wander pattern measured from actual aircraft operations. The traffic distribution was purposely centered over successive mat joints to ensure the most damaging effect, in terms of fatigue loading, across the center and each side of the 61-cm (24-in.) longitudinal mechanical joints welded to the panel ends. Failure of the full-

scale test section was defined as either the formation of 3.18 cm (1.25 in.) of subgrade deformation underneath the mat system or breakage of individual mat panels that required replacement of 10 percent of the traffic area.

Figure 9. AM2 matting panels trafficked by aircraft simulator in full-scale test section.

In the full-scale experiments presented in this paper, failure occurred after four panels had become severely damaged and were considered hazardous to the load wheel of the aircraft simulator. The aircraft simulator was equipped with a single-wheel loaded to 156.73 kN (35,235 lbf) with an internal tire pressure of 2.24 MPa (325 psi). The tire contact area was approximately 703 cm^2 (109 $in.^2$) and the width of the loaded area was approximately 22.9 cm (9 in.). The wander pattern resulted in five adjacent traffic lanes with the outer two lanes receiving 50 percent of the number of cycles of the center three lanes. Figure 10 shows the wander pattern and traffic distribution in relation to the location of the mat joints.

3.6 Results of full-scale experiments

The five full-scale test sections were all trafficked until a minimum of four individual panels (10 percent of the trafficked area) had failed by fatigue, resulting in overall failure of the system as defined by the researchers. The failure criterion of 10 percent mat breakage was determined by research stakeholders to allow for a “reasonable” amount of maintenance on an operational airfield. The labor and materials required to replace some of the AM2 mat panels are expected to be available; however, failures of greater than 10 percent of the surfaced area may result in unsustainable maintenance requirements and in unacceptable windows of airfield surface closure. The reader should note that “failures” of AM2 mat panels do not happen abruptly. The AA60601 material is ductile, and panel damage can be observed well before the panel becomes inoperable.

Figure 10. Traffic distribution pattern
in full-scale test section.

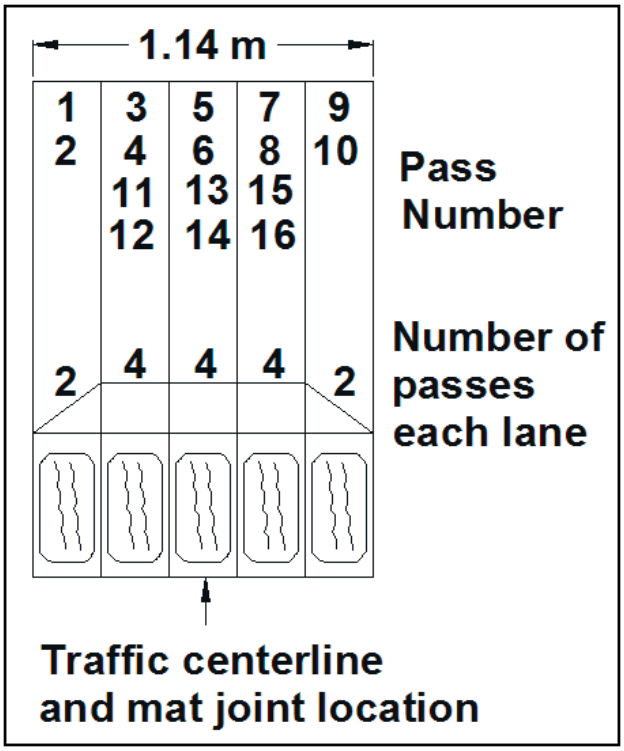

Figure 11 presents the number of cycles to failure for the first and fourth panel (system) failures for each of the five full-scale experiments. Most of the individual panel failures over CBRs of 6, 10, 15, and 25 percent occurred in an area of shear and high tensile stress concentration along a narrow cross section of the overlap/underlap joint (shown as region 1 in Figure 12b), resulting in complete removal of the upper underlap component of the joint as depicted in Figure 13. The combination of shear and tensile stresses occurred when the load was applied on the right side of the joint shown of Figure 12b, and the locking bar applied a vertical force on the upper underlap tab. The translation of the underlap side of the joint caused the locking bar to only contact the left edge of the upper underlap tab and did not uniformly transfer load along the tab. The result was an induced moment at region 1 in Figure 12b that caused bending, yielding, and ultimately low-cycle induced fatigue cracking in region 1 in Figure 12b that propagated along the length of the tab until it completely separated from the joint.

Figure 11. Mat breakage fatigue results for first panel and system failures.

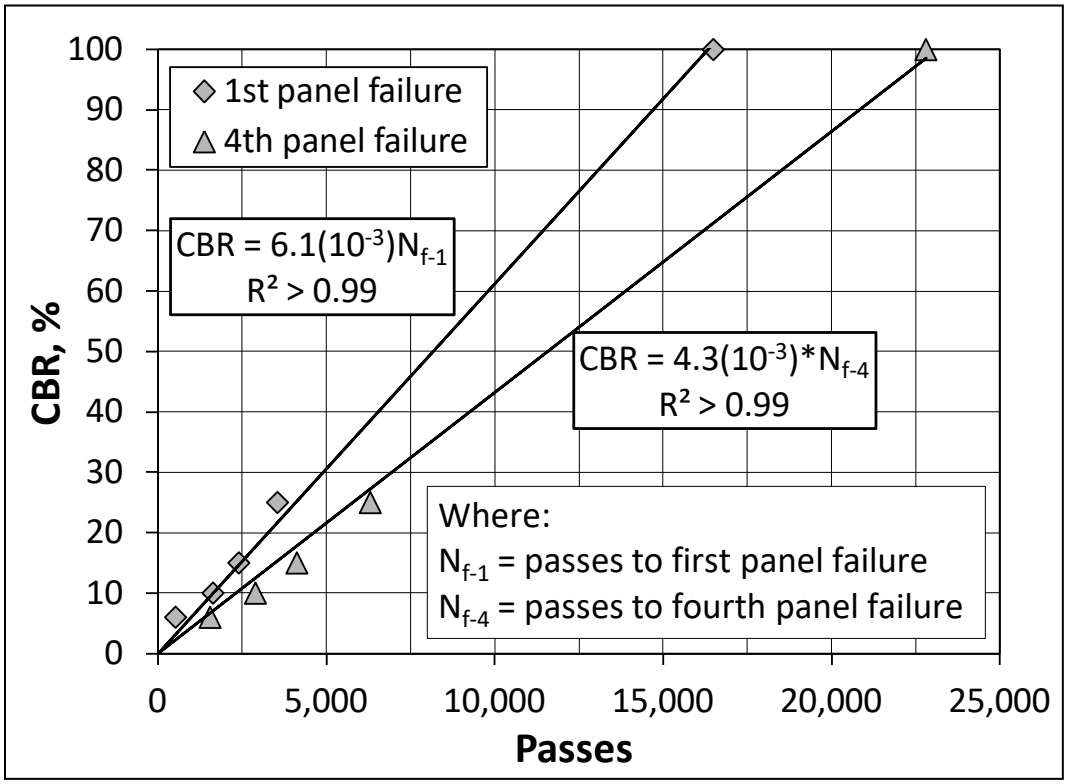

Figure 12. Laboratory test fixture (a) Laboratory test boundary conditions, (b) Areas of stress concentration in laboratory experiment (not to scale), and (c) Photo of experimental laboratory test fixture.

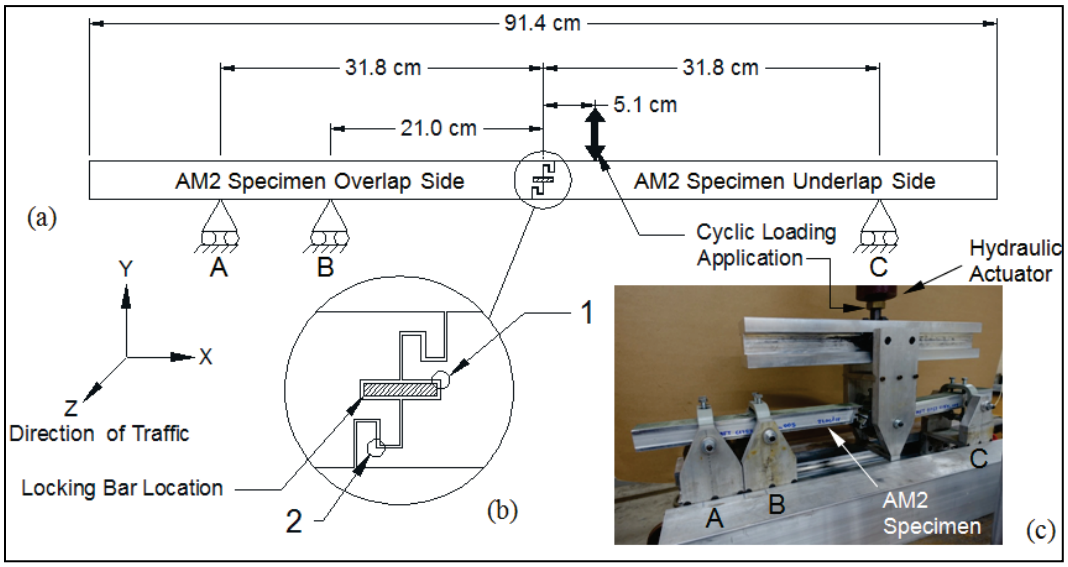

Figure 13. Typical separation of fatigue critical component from AM2 style mat joint.

The number of passes to fatigue failure was directly related to the rate of formation and the magnitude of plastic deformation (rut formation) in the subgrade. Since subgrade conditions with low CBRs deform faster than those with higher CBRs, the number of cycles required to cause individual panel fatigue failures also increased with CBR. When the mat system was evaluated over a CBR of 25 percent, the failure location began to move from the mechanical connectors along the welded 61-cm (2-ft) panel ends to the internal structure of the mat. When placed over a CBR of 100 percent, nearly all failures were internal. The changing failure location was a result of the lack of subgrade deformation and, therefore, reduced movement of the end connector joint. Without movement, the load was transferred directly through the core of the mat panels without inducing enough stress/strain to cause fatigue in the critical stress location of the end connector joint.

Since the objective of the study was to develop a model to predict fatigue failure in the AM2 mat system, the data in Figure 11 were analyzed to determine the best method of constructing a model. Surprisingly, the trends for both the first panel failure and the fourth panel (system) failure are nearly linear, as shown in the best fit equations in Figure 11 with coefficients of determination, $R^2 > 0.99$. Therefore, prediction of the number of cycles to failure for any given subgrade CBR under the tested load condition can be determined by using a linear relationship. To predict the first panel failure or overall system failure (when defined as 10 percent mat panel breakage based on the reasons discussed in the first paragraph of

this section), Equations 4 and 5 were derived from Figure 11 where *CBR* = the CBR of the subgrade, $N_{f\text{-}1}$ = number of aircraft passes causing the first panel failure in the field experiments, and $N_{f\text{-}4}$ = number of aircraft passes causing system failure in the field experiments. The equations can be solved for CBR to be used as a design tool to determine the minimum CBR required to meet a mission requirement in terms of passes to the first panel failure, Equation 4 or overall system failure, Equation 5. Conversely, these equations can be solved for *N* to be used as a site evaluation tool so that planners can predict the number of allowable passes prior to the chosen failure condition.

$$\frac{CBR}{N_{f-1}} = 6.1\ x\ 10^{-3} \tag{4}$$

$$\frac{CBR}{N_{f-4}} = 4.3\ x\ 10^{-3} \tag{5}$$

The determination of the appropriate model to use requires further discussion. The full-scale experimental test program was designed as a worst-case condition that likely cannot be replicated in service. The simulated aircraft was chosen as the most damaging load in the U.S. military inventory. The tire pressure of 2.24 MPa (325 psi) is much higher than most other aircraft, and the simulator was loaded to the maximum allowable gross load resulting in 156.73 kN (35,235 lbf) on a single wheel. The only way this load can be achieved is for the aircraft to carry a maximum payload and be completely full of fuel. In reality, the majority of the traffic on an airfield will be much less severe to the AM2 mat surface. Additionally, the traffic pattern was intentionally centered over a row of alternating 61-cm (2-ft) end connector joints to induce the most fatigue damage to the mechanical connectors. In reality, airfields experience a variety of aircraft types, each with a unique spacing between the main landing gears. Therefore, the likelihood of traffic being concentrated over a row of mat joints is small. The inherent conservatism in the factors used to derive the models likely gives more merit to the use of the system failure model for normal operation use and is recommended to the stakeholders. However, if either labor or material supplies prohibit major maintenance activities on the airfield, the ultraconservative first panel failure prediction model may be considered.

3.7 Laboratory experiments

To reduce the cost of full-scale experimentation (and to be able to efficiently test alternate joint designs), the authors desired to develop a laboratory fixture and procedure to mimic fatigue failures observed in the field. Several iterations of experiments were attempted before a representative method was discovered. Initial attempts included varying the boundary condition (e.g., supporting joints with rubber representing the subgrade soil's stiffness) and loading type (constant load amplitude and variable load amplitude). In these early attempts, the loading location was varied, but the amount of displacement could not be controlled, and the fracture location of the sample was not representative of the full-scale experiment fracture location.

After further inspection, researchers began experimenting with laboratory configurations using cantilevered beams in attempt to isolate the load in the upper underlap tab that was observed to fail in field experiments. Researchers discovered that failures in the critical stress location (region 1 in Figure 12b) would occur only in the laboratory experiments when the loading was applied to the underlap side of the joint while holding the overlap side relatively constrained, and very little (or no) damage occurred when the load was applied to the overlap side. In an actual assembly (and in the full-scale experiments), the system is rigid enough to prevent most joint rotation. While the applied load is predominately shear, due to the rotation of the locking bar, the resultant load transfer from one panel to the adjacent panel results in significant local bending stress of the upper underlap tab. This dominant local bending stress instead of shear loading is reasonable when considering the interaction of the locking bar and the joints. When load was applied, the relatively large tolerances built into the joint to allow for assembly of a panel array allowed for vertical translation of the underlap side of the joint prior to contact with the locking bar. This caused the locking bar to rotate and contact the upper underlap tab only on the left edge, thus causing bending about region 1, as shown in Figure 12b.

Researchers also realized that the subgrade deformation greatly influenced the movement and amount of load transfer through the joint and the amount of joint movement increased with each pass of the load wheel because of the subgrade deformation. Rushing and Howard (2015) used the same full-scale data set presented in this paper to predict the subgrade deformation for various subgrade CBRs. To accurately predict fatigue in

the joints, the discovery of the loading location required to cause the expected joint fatigue damage was coupled with the subgrade deformation prediction model to develop an increasing amplitude displacement controlled experiment. The following paragraphs describe the displacement function derivation, laboratory experimental test set-up, boundary conditions, and the applied load calibration.

A laboratory procedure was designed to use the subgrade deformation model, Equation 6 derived by Rushing and Howard (2015) and programmed as an increasing amplitude displacement function using an MTS Systems Corporation hydraulic actuator, control system, and data acquisition system. The required loading range for this experiment was 0 to 22 kN (5,000 lbf) with a loading rate of 0.5 Hz. The data acquisition rate was set at 51.2 Hz. Time, load, and displacement were recorded continuously throughout the experiments.

$$\delta_s = log_{10}P_n \cdot 1.64 \cdot CBR^{-0.61} \quad (6)$$

In Equation 6, δ_s = the subgrade deformation, in., P_n = the number of passes, and *CBR* is the CBR of the subgrade underneath the structural mat system. To validate the laboratory experiment, CBR's of 6, 10, 15, 25, and 100 percent were used to calculate δ_s using Equation 6 from P_n = 1 to 10,000 as shown in Figure 14 (left axis) to match the CBR values of the full-scale experiments.

Researchers also realized that in order to simulate conditions in the lab, the geometries required for full-scale deformation would not be practical in the lab. During field experiments, the width of subgrade deformation, W_{field}, measured approximately 1.22 m (4 ft) since the traffic was applied over a 1.14-m- (45-in.-) wide area as shown in Figure 10, and 3.18 cm (1.25 in.) of downward movement, D_{field}, was required to rotate the end joints far enough for the area in region 2 in Figure 12b to be affected. Because the full-scale tests were concluded at or shortly after 3.18 cm (1.25 in.) of subgrade deformation had developed, failures in this region were not observed. Since the outer constraints in the laboratory test set up were 62.23 cm (24.5 in.) apart, w_{lab}, the vertical displacement, d_{lab}, required to develop the same angle of rotation in the joint was determined by solving the ratio

$$\frac{D_{field}}{W_{field}} = \frac{d_{lab}}{w_{lab}} \quad (7)$$

where d_{lab} = 1.63 cm (0.64 in.) (To maintain a consistent rotational degree in the laboratory experiments, the programmed displacements calculated using Equation 6 were multiplied by $\frac{d_{lab}}{D_{field}}$ = 0.5 as shown in the secondary y-axis in Figure 14.

Figure 14. Field and laboratory displacement prediction models.

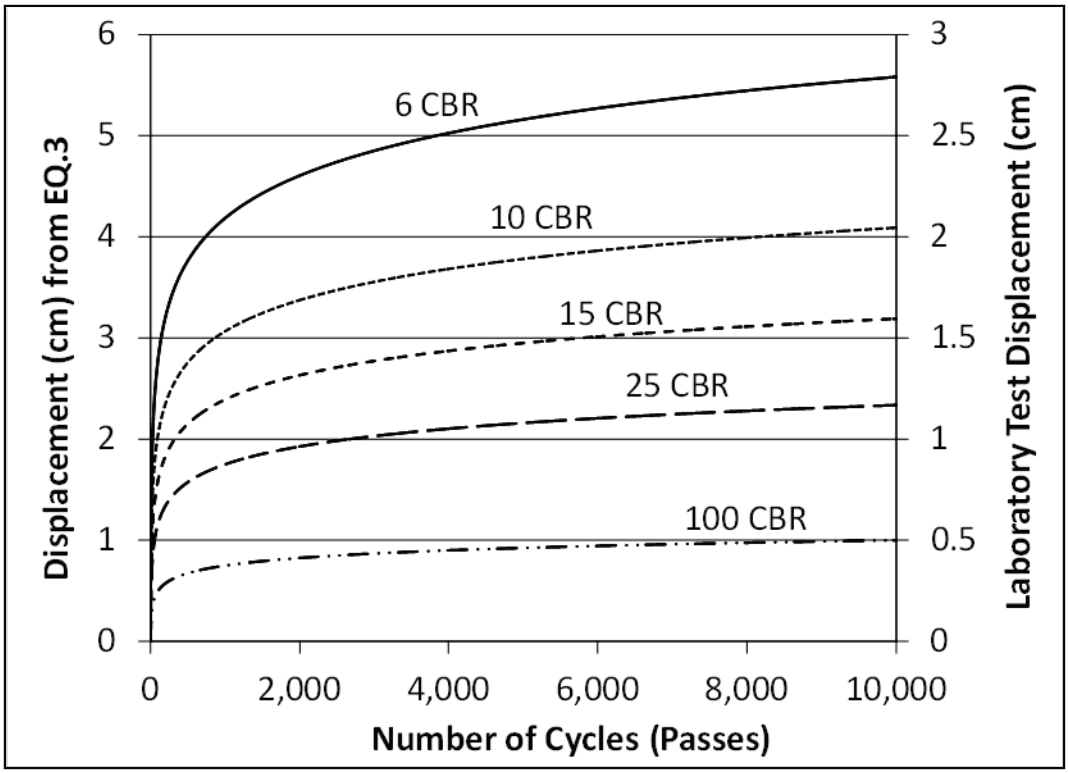

Laboratory test specimens consisted of 5.1-cm- (2-in.-) wide sections of matting cut across the 61-cm (2-ft) welded fatigue critical joint that were 45.7 cm (18 in.) long on each side of the joint centerline. Once the joint was assembled and a locking bar was inserted to prevent vertical separation of the joint, the entire sample was approximately 91.4 cm (36 in.) long. A custom test fixture was designed to closely mimic boundary conditions thought to exist in the field experiments as shown in Figures 12a and 12c. Each constraint and loading location was constructed as a section of a box beam with set screws on the top and bottom that sandwiched the sample and held it in place. Pins were used to allow the box beam section to rotate freely, and a track system and bearings were designed to allow for freedom of horizontal movement. The underlap side of the joint was constrained only in the vertical direction 31.8 cm (12.5 in.) from the joint centerline as shown in Figure 12a. The increasing amplitude cyclic displacement was applied 5.1 cm (2 in.) from the underlap end of the joint

using a fixture identical to the other constraints so that a downward displacement could be applied and then return the sample to the original vertical position. The overlap joint was fixtured as a cantilever beam, as shown in Figure 12a, constrained only in the vertical (Y) direction at two locations. These two constraints were also pinned rollers as described above for the underlap side of the joint. The first and second constraint locations were 31.8 cm (12.5 in.) and 21 cm (8.25 in.), respectively, from the joint centerline.

The test fixture was calibrated by moving the location of the interior constraint (shown in Figure 12a) on the cantilevered side of the joint until a 13.34 kN (3,000 lbf) applied vertical load was required to displace the sample 1.59 cm (0.625 in.) downward (i.e., the failure displacement calculated by multiplying 3.18 cm (1.25 in.) of field displacement by $\frac{d_{lab}}{D_{field}} = 0.5$). The calibration method was chosen to best represent the conditions experienced by the joint from the full-scale experimentation. In the full-scale experiments, the aircraft load was 156.73 kN (35,235 lbf) and the actual end connector joint is about 57.15 cm (22.5 in.) long. Assuming the entire load is transferred through the joint, approximately 2.7 kN/cm (1,500 lbf/in.) should be considered. Since the laboratory specimens were 5.08 cm (2 in.) wide, a maximum load of about 13.34 kN (3,000 lbf) should occur prior to the rotational limit of 1.59 cm (0.625 in.). This calibration method ensured the sample failed in the fatigue critical zone, shown as region 1 in Figure 12b, that was observed in the majority of failures in the full-scale experiments. Preliminary laboratory test configrations showed that if the applied vertical load exceeded 13.34 kN (3,000 lbf) prior to achieving a displacement of 1.59 cm (0.625 in.) the sample would fail prematurely in comparison to full-scale observations. If the load was less than 13.34 kN (3,000 lbf) prior to displacement of 1.59 cm (0.625 in.), the sample would rotate further than field constraints allowed and the joint would fail in region 2 in Figure 12b. The CBR of 6 percent test program was used to calibrate the sample, and the three constraint locations were repeated for all other experiments.

3.8 Results of laboratory experiments

The results of the laboratory experiments in terms of number of cycles to failure are shown in Figure 15 for simulated CBR values of 6, 10, 15, and 25 percent (16 total tests). The sample set includes five replicates tested under simulated CBRs of 6, 10, and 15 and one at 25 percent. Researchers

focused their efforts on the predictability of the lower CBR values because full-scale experimental results indicated the failure mechanism would shift to the core of the panel as the subgrade deformation decreased from elevated CBR values.

Figure 15. Results of laboratory fatigue failures.

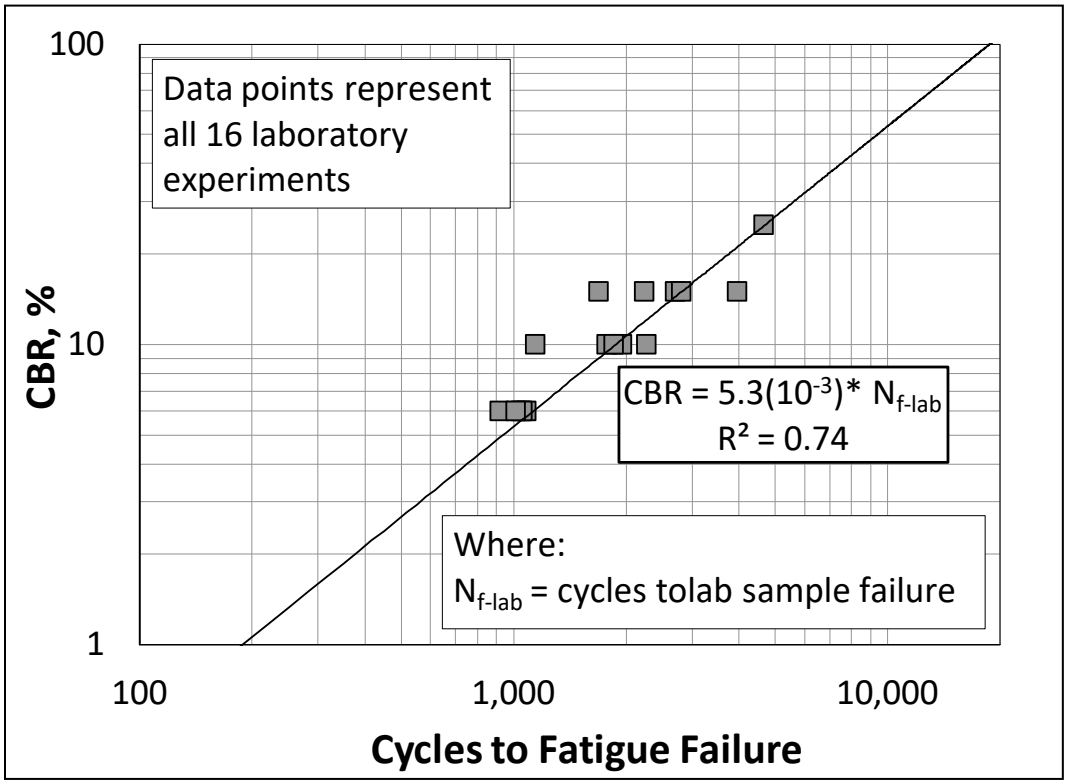

Meaningful scatter can be observed in the data presented in Figure 15. The scatter is thought to be the result of asymmetrical loading across the sample joint caused by movement of the locking bar in its slot during testing causing the exact point of loading during each successive cycle to be unpredictable. To test this hypothesis, researchers affixed adhesive bonded foil strain gauges to symmetric locations on the fatigue critical locations of the joint near the failure point indicated by region 1 in Figure 12b as shown in Figures 16a and 16b with results typical of those shown in Figure 16c. Significant variability was noted; researchers realized that the strain gradient across the narrow cross section from the tension to compression face was meaningful. The large strain gradient made accurate, symmetric, measurement very difficult since perfectly symmetric placement of the gauges on the scale required for valid measurement was not possible. Successive attempts did not give repeatable results, so the test lacked the fidelity for this spatial distribution and would require high

magnification digital image correlation (or equivalent) to capture the actual strain gradients of the material. Furthermore, validation of the strain response by the addition of strain gauges in similar locations on the mats in the full-scale tests was not possible without degrading the integrity of the panel's structure. While this approach could have given additional merit to the laboratory procedure, it was not feasible.

The freedom of the test specimens to move horizontally likely led to further changes in the location of load concentration throughout the test. However, since the goal of the laboratory experimentation was to mimic field conditions as closely as possible, this level of movement during the test was expected and is reasonable. From the test results in Figure 15, Equation 8, represents the data with a reasonable R^2 of about 0.74, where $N_{f\text{-}lab}$ is the number of cycles required for joint failure in the laboratory experiment and *CBR* is the programmed subgrade bearing capacity. The best fit line falls directly between the first and system failure models derived from the full-scale experimentation results and shown in Equations 4 and 5.

$$\frac{CBR}{N_{f-lab}} = 5.3\ x\ 10^{-3} \quad (5)$$

To compare the scatter of the laboratory and full-scale experiments, the full-scale experimentation data was normalized to account only for loading cycles that occurred on the underlap side of the joint. Since the location of the test wheel during the experiments was approximate, only the 4 passes directly over the joint and the 6 passes in the two lanes on the underlap side of the joint, 10 of the 16 passes required to complete the pattern shown in Figure 10, were included in the analysis. Therefore, the number of cycles required for the first, $N_{f\text{-}1}$, and fourth, $N_{f\text{-}4}$, panel failures during the full-scale experiment were multiplied by 0.625 (or 10/16) as shown in Figure 17. The resulting values ($N_{f\text{-}1}$ and $N_{f\text{-}4}$) for each tested CBR were plotted with their matching pairs (minimum and maximum failure values) from the laboratory experiments ($N_{f\text{-}lab}$) to assess scatter. With the exception of a single data point from $N_{f\text{-}1}$ observed in the CBR of 6 percent full-scale experiment, all comparisons fell encouragingly near the line of equality. Further investigation revealed the one data point away from the equality line may have been an outlier.

Figure 16. Strain measurement attempts on laboratory specimens (a) Image of installed strain gauge prior to failure with locking bar loading, Upper underlap tab at critical stress location, (b) Image of strain gauge after failure at critical stress location, and (c) Strain measurements at symmetric locations on both sides of a test specimen showing highly variable results.

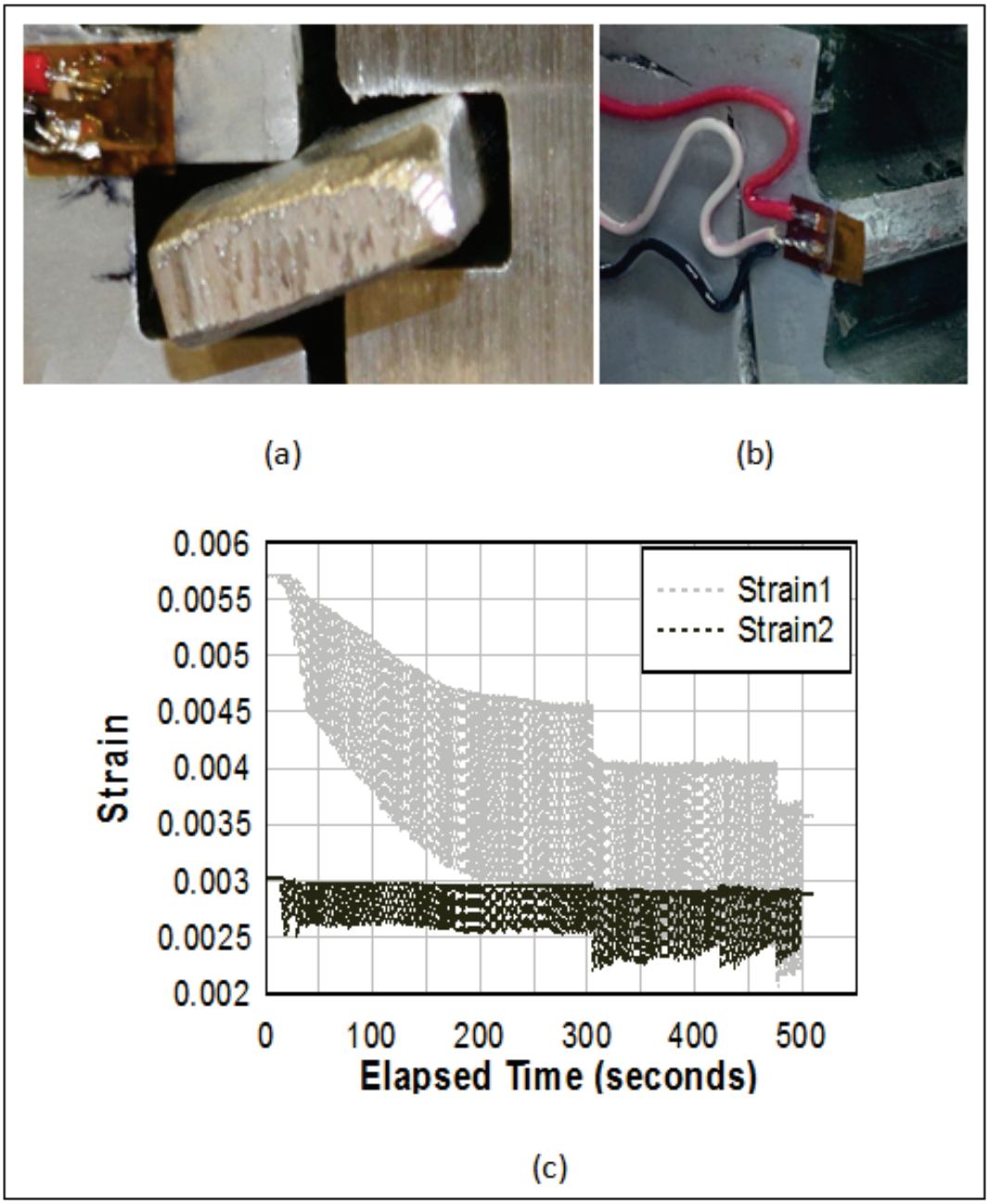

Figure 17. Comparison field and laboratory experiments based on minimum and maximum number of cycles to failure at a given CBR.

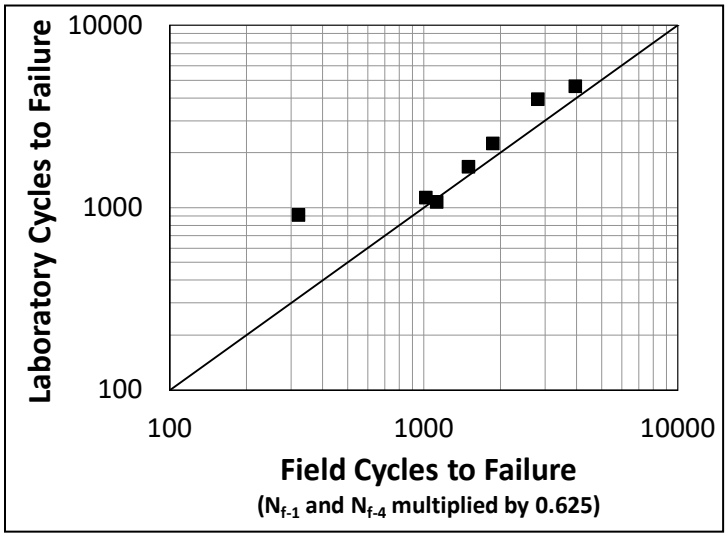

To further compare the data, the average laboratory experimental values were plotted with the overall system failure numbers from the full-scale experiments (Figure 18). The results for the CBRs of 6, 10, and 15 percent were near perfect matches and the CBR of 25 percent fell very near the line of equality. The data provides considerable evidence that the designed laboratory loading procedure and boundary conditions presented herein are truly representative of the actual conditions that occur in the field for a single-wheel load configuration. Using this procedure, data available to date suggests users can reasonably estimate the number of cycles required to induce fatigue failure in the AM2 joint in the laboratory.

Figure 18. Comparison of full-scale system failure and average failure from laboratory experiments at a given CBR.

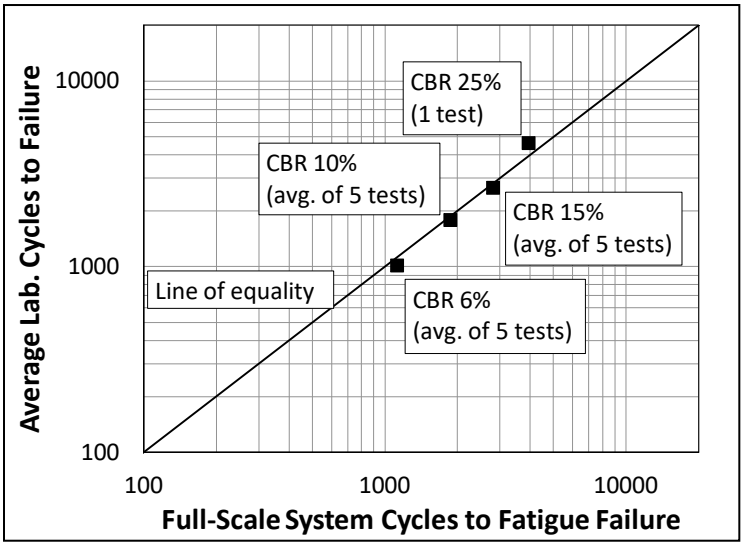

3.9 Discussion of results

The ability to characterize and quantify the fatigue performance of airfield mat joints (AM2 or other mat designs) in a laboratory investigation has the potential to save considerable full-scale test-section costs by eliminating inferior designs from consideration, thus reducing the risk of premature field failures. With the constant evolution of lightweight materials and aircraft loadings, considerable future efforts are expected to evaluate lighter materials and optimized joint designs to reduce the logistics required to deliver airfield matting. This paper's findings can be used to simulate field conditions in a laboratory setting and evaluate new materials and designs in a cost-effective procedure. A process similar to the one described in this paper could also be designed to replicate fatigue of other structural systems placed over a deformable media as long as the boundary conditions can be replicated in a laboratory. With the ability to friction stir weld dissimilar aluminum alloys, researchers are interested in changing the material type of the 61-cm (2-ft) AM2 end connector joint to a harder alloy and friction stir welding it to the AA6061 hollow core extrusion to reduce fatigue damage in the joint. This approach has been successfully implemented with similar alloy combinations for hollow core extrusions such as rail-car bodies as described by Kawasaki et al. 2004. The authors have recently characterized similar and dissimilar aluminum alloy combinations (Rodriguez et al. 2015, 2016) and have designed and fabricated new prototype mat panels using friction stir welding to attach the panel's end connectors. The authors of this chapter's content intend to use the laboratory procedure presented herein to show the feasibility and potential for cost reduction and improved durability using alternative designs and manufacturing methods. The designed laboratory procedure offers a relatively inexpensive method to experimentally quantify the improvement of fatigue life when using new materials or alternative joint designs.

3.10 Summary and conclusions

Full-scale simulated aircraft tests were conducted over the AM2 aluminum matting system installed over CBRs of 6, 10, 15, 25, and 100 percent to determine the number of simulated aircraft passes required to cause fatigue failure of the mechanical joints used to assemble the panels. The data was analyzed, and two models were created using the results that are capable of predicting either the first panel failure, $N_{f\text{-}1,}$ or the overall mat system failure, $N_{f\text{-}4,}$ with a high degree of certainty for placement of AM2 over any subgrade support condition under the loading conditions tested.

These models can be used to determine the subgrade strength requirement to meet a mission requirement or to predict the number of passes to failure based on an existing subgrade condition. A subgrade deformation model developed by the authors was used to create an increasing amplitude function that replicated the amount of displacement experienced by the mat joint from the full-scale experiments. This function accounted for accumulated damage, or permanent deformation, of the subgrade and increased the displacement of the joint with each successive cycle. A laboratory test fixture was designed to replicate the field boundary conditions. The results of the laboratory experiment showed strong correlation between the field and laboratory data, thus supporting its ability to predict field failures at a fraction of the cost of full-scale test section construction and execution.

The fatigue model presented in this paper is part of a larger effort consisting of three major emphasis areas: the development of a model to predict subgrade deformation as described by Rushing and Howard (2015), the development of a model to predict fatigue failure of the mat as a function of vertical displacement (based on the subgrade deformation model) and number of applied load cycles (described herein), and the creation of a design and evaluation framework used to determine the subgrade strength required to support a specified number of aircraft passes or to determine the number of allowable aircraft passes for a given subgrade strength.

3.11 Acknowledgements

The full-scale and laboratory experiments and resulting data presented in this chapter were obtained from research conducted at the U.S. Army ERDC, Geotechnical and Structures Laboratory (GSL), Airfields and Pavements Branch with funds provided by the U.S. Air Force Civil Engineer Center (AFCEC) and the office of the Assistant Secretary of the Army for Acquisitions, Logistics, and Technology (ASAALT). The sponsors determined the scope of the study but did not assist in data collection, analysis, or writing. The support of AFCEC, ASAALT, and ERDC personnel is gratefully acknowledged. A special thank you goes to Jeb Tingle, Quint Mason, Tim McCaffrey, and Lyan Garcia, of the ERDC GSL, who were instrumental in the successful completion of this research. Permission to publish this work was granted by the Director, Geotechnical and Structures Laboratory.

4 Analysis of AM2 Airfield Matting Performance under Six-Wheel Boeing C-17 Gear Loading

This chapter represents the final draft of an article that has been published by ASTM International in the *Journal of Testing and Evaluation*. The as-published article can be accessed using the following internet address: http://dx.doi.org/10.1520/JTE20160255. The draft article (Rushing and Howard 2017) has been reformatted and reproduced herein with minor modifications to meet the formatting requirements of this report following the permission guidelines published by ASTM International.

4.1 Abstract

Methods previously developed to predict the performance of AM2 aluminum airfield matting subjected to single-wheel aircraft loads were evaluated in this paper to determine their validity for the complex six-wheel Boeing C-17 main landing gear. These methods, derived from full-scale accelerated F-15E trafficking, were used to predict deformation of the subgrade as a function of the California bearing ratio (CBR) and the number of aircraft passes. The same data set was also used to predict fatigue failure of the mat system's joints over any CBR. A laboratory test fixture and procedure were designed to mimic the boundary conditions experienced by the mat during full-scale experiments (single-wheel F-15E in the original experiments) so that variations of the joints and any subgrade CBR can theoretically be tested in fatigue without the expense of full-scale experiments. Results presented in this paper showed that, even with a more complex loading configuration (i.e., C-17), the trends published previously for the F-15E were supported, and the procedures offered reasonable predictions for AM2.

4.2 Introduction

The ability to expand and create temporary aircraft operating surfaces using structural matting systems began in the late 1930s with the advent of modern aircraft. Early matting systems were made of wood and were primarily used in Europe. As aircraft weights and tire pressures rapidly increased, new designs were required to be stronger and more durable. Early versions were made from steel, but as aircraft evolved, the section modulus required to resist deformation led to the predominant use of

extruded aluminum to reduce transportation logistics. Although temporary by design, airfield matting installations function as pavement systems and require design and evaluation procedures to predict performance under field conditions. The underlying subgrade on which the mat is placed must be strong enough to resist excessive deformation for the design traffic condition, and the mats themselves must resist damage from low-cycle fatigue in their structural core and fastening systems. Planners and operators of the systems must be able to estimate the usable life of an installation similar to the way flexible or rigid pavements are designed and evaluated. To improve this process for the current AM2 matting system, described in the section titled "AM2 Matting" below, an accelerated testing and evaluation program was initiated to monitor AM2's performance under simulated F-15E and C-17 aircraft loads.

4.3 Objective and scope

The objective of the work described in this paper was to analyze the data collected from full-scale accelerated AM2 mat tests subjected to simulated Boeing C-17 aircraft traffic to develop relationships to predict the subgrade deformation and AM2 mat fatigue damage for any subgrade condition. The objective was accomplished partially by utilizing procedures previously derived by Rushing and Howard (2015) and Rushing et al. (2016) for single-wheel F-15E loadings. Specifically, this paper describes (1) development of an equation to predict subgrade deformation under the Boeing C-17 aircraft on AM2 matting, (2) development of an equation to predict AM2 fatigue damage when subjected to repeated Boeing C-17 loadings, and (3) evaluation of a novel increasing amplitude laboratory procedure to predict low-cycle field fatigue performance for any subgrade condition. The work described in this paper evaluates the validity of one of the authors' previous works for one of the most complex aircraft gear configurations in existence (C-17).

The scope of this study includes (1) a detailed literature review, (2) a series of four full-scale accelerated aircraft traffic tests conducted on controlled test sections surfaced with AM2 matting with California bearing ratios (CBRs) of 6, 10, 15, and 25 percent, and (3) increasing amplitude displacement controlled laboratory experiments conducted using data collected from the full-scale experiments as inputs.

4.4 Literature review

4.4.1 Airfield matting predictions

A literature review found that researchers at the Waterways Experiment Station (WES) in Vicksburg, MS (now the U.S. Army Engineer Research and Development Center or ERDC) began publishing studies on the prediction of airfield mat behavior in the 1950s. A comprehensive literature review was conducted by Rushing and Howard (2015) and Rushing et al. (2016) on airfield mat performance prediction. A summary of this work is presented in Table 5.

4.4.2 Prediction of subgrade deformation under vehicle traffic

The Boeing C-17 aircraft was designed to operate on unsurfaced airfields; therefore, the gear is robust and can handle subgrade deformations of up to 7.6 cm (3 in.) underneath the mat surface. Deformations of this magnitude begin to deviate from traditional airfield pavement failures and shift more toward off-road mobility behavior. Literature was reviewed to identify existing models that predict large soil deformations under heavy loads that might be useful for studying C-17 trafficking.

Li and Selig (1996) refined a commonly used plastic strain power model, $\varepsilon_p = AN^b$, defined by Monismith et al. (1975), to predict plastic strain, ε_p, based on the number of repeated load cycles, N, and two coefficients A and b, that were dependent on soil type, soil properties, and stress state. Coefficient b was found to be independent of the deviator stress and soil properties and was determined as the slope of the line resulting from a plot of N and cumulative ε_p. However, b was found to be meaningfully different for different soil types. Coefficient A = soil ε_p after $N = 1$ and was therefore dependent on the soil type, soil physical properties, and the deviator stress as described in Equation 9:

$$A = a\left(\frac{\sigma_d}{\sigma_s}\right)^m \tag{9}$$

where a and m are material parameters, and σ_d is the deviator stress; σ_s is the soil static strength. The authors of the content of this chapter admitted that factors a, m, and b were difficult to determine by simple tests and required sophisticated repeated loading tests. To assist future studies, a table of typical ranges of these factors, reproduced in Table 6, was included in their research.

Table 5. Literature review of airfield mat performance prediction work from 1951 to 2016.

Reference	Matting Type	Soil Strength	Vehicle Type	Key Findings
Pickett (1951)	All metal airfield mats available (i.e., pierced steel plank)	Attempted for all soil CBRs	Stress based, all available aircraft, (i.e., B-17, B-24)	Mats were approximated as thin membranes of infinite extent supported on a liquid subgrade incapable of supporting shear stresses.
Pickett (1955)	All metal airfield mats available (i.e., pierced steel plank)	Attempted for all soil CBRs	Stress based, all available aircraft,(i.e., B-17, B-24)	Mats were approximated as orthotropic mats over elastic subgrades. The direction of the mat perpendicular to traffic required the most rigidity, and mat deflections were reduced by increasing the strength of the subgrade.
Harr and Rosner (1969)	All metal airfield mats available	Attempted for all soil CBRs	Stress based, F-4, and all available aircraft	Airfield mat joint efficiencies can be back calculated from full-scale test data for more advanced analysis; however, the end joints were found to be 10-16 percent less effective for moment transfer than interior mat elements and must be considered for modeling and analysis.
White (1971b)	All metal airfield mats available	Attempted for all soil CBRs	Stress based, all available aircraft	Even the most sophisticated models were unable to truly characterize matting performance, and computational advances are needed for advanced analysis using Finite Elements (FE).
Berney et al. (2006)	Various, including AM2, M-19, composites, etc.	NA, in-air tests	NA, in-air tests	Developed a method to use 2-D FE analysis to back-calculate the flexural rigidity of mats using full-panel 4-pt bend tests.
Gartrell (2007)	Various composites including Durabase and ACE-mat	Varied 4, 8, and 40 percent	C-130 and C-17	Joints were accounted for by varying load transfer percentages between panels, but models could not account for accumulated damage nor rutting in the subgrade from repeated loading.
Gonzalez and Rushing (2010)	Various	4, 6, 8, 10, and 15 percent	C-130, C-17, and F-15E	Developed a mechanistic-empirical model using layered elastic theory to relate subgrade deviator stress, CBR, and aircraft coverages to failure, but did not consider joints.
Rushing and Howard (2011)	Various	1, 5, 15, and 80 percent	7-Ton Truck	Developed prediction relationships for subgrade deformation based on full-scale test section data.
Doyle et al. (2014)	Composites	4, 8, and 40 percent	C-130, C-17	FE analysis can be used to rank mat performance based on approximating flexural rigidity across the joints, but work is needed to characterize joint behavior.
Rushing and Howard (2015)	AM2	6, 10, 15, 25, and 100 percent	F-15E	Developed a method to predict subgrade deformation for AM2 subjected to F-15E loadings based on full-scale accelerated test data.
Rushing et al. (2016)	AM2	6, 10, 15, 25, and 100 percent	F-15E	Developed a method to predict mat fatigue damage as a function of subgrade CBR and number of passes for the F-15E. Developed a laboratory fixture and method to replicate the subgrade deformation and predict joint damage for AM2.

Table 6. Average model parameters suggested by Li and Selig (1996).

	Soil Classification			
Model parameters	ML	MH	CL	CH
a	0.64	0.84	1.10	1.20
b	0.10	0.13	0.16	0.18
m	1.70	2.00	2.00	2.40

Chai and Miura (2002) further refined the work of Li and Selig (1996) by adding another term to their proposed equation and a fourth constant, n, as shown in Equation 10:

$$\varepsilon_p = a(\frac{\sigma_d}{\sigma_f})^m(1 + \frac{\sigma_s}{\sigma_f})^n N^b \quad (10)$$

where σ_f = static strength of the soil, σ_s = initial deviator stress, and n = 1.0 was suggested to represent most soil conditions. The authors re-defined a so that $a = \alpha C_c$, where α was back-calculated as approximately 8.0, and C_c was the soil compression index. The initial deviator stress, σ_s, was calculated through the use of 2-D finite element analysis or by complex hand calculations.

Although the Li and Selig (1996) and Chai and Miura (2002) models considered cumulative plastic strain (permanent deformation) in the subgrade, they did not consider loadings of the magnitude of those applied by heavy aircraft such as the C-17 and still require empirical data to determine their controlling factors.

Jones et al. (2005) presented a complex model used by U.S. military and North Atlantic Treaty Organization (NATO) to predict large subgrade deformations caused by military vehicles based on a Rating Cone Index, RCI, that measures the penetration resistance of a standard cone when pressed into in situ soil. Vehicle and tire characteristics are then added, and the resulting deformation of the soil can be predicted. Hambleton and Drescher (2008) used 3-D finite element analysis to predict subgrade deformation under vehicle traffic for both clay and sand soils. Their model was complex but only considered the effect of a single load application. Because neither of these models accounted for damage accumulation under repeated load cycles, they were not applicable to predicting deformation underneath a matted surface.

Vahedifard et al. (2016) and Vahedifard et al. (2017) assembled a database of thousands of off-road mobility algorithms for sand and clay soils to evaluate numerous parameters such as sinkage. The database is referred to as DROVE (Database Records for Off-Road Vehicle Environments). DROVE is not suitable for C-17 loading.

Garcia (2015) compared six unique matting systems, including AM2, to develop an expedient tool to approximate the subgrade deformation, δ_s, underneath the mat based on the number of loading cycles and the composite modulus of the mat system, E_c^{NJ}, absent the joints as shown in Equation 11

$$\delta_s = log_{10}P_n * 686.26 * (E_c^{NJ})^{-0.63} \quad (11)$$

where P_n = number of passes. The prediction equation was developed specifically for an F-15E aircraft traffic load application over a CBR of 6 percent. The F-15E was chosen because of the extent of near-surface damage caused by its high tire pressure and small loading area. The CBR of 6 percent was the minimum allowable subgrade strength requirement chosen for airfield matting applications. This procedure was developed as a selection tool to determine if a matting system was a viable option for F-15E operations but was not intended to predict C-17 performance.

4.4.3 Low-cycle fatigue prediction of in-service aluminum transportation structures

ASTM E606/E606M (ASTM 2012) is the primary standard for strain-controlled fatigue testing. ASTM E606 is intended for specimens and is not intended for testing of full-scale components (i.e., AM2 joints). It is used primarily to determine material properties to support research and mechanical design. Prior to Rushing et al. (2016), a standard test could not be located by the authors to characterize the complex in-service conditions experienced by a mat joint. Kaisand and Mowbray (1979) developed relationships between low-cycle fatigue and fatigue crack growth rate properties for metals, but their approach was also limited to specimens (not components of systems such as AM2). Zwerneman and Frank (1988) considered fatigue damage under variable amplitude loads to describe in-service effects of vehicle loads on bridge components. They found that the complex cycles experienced by the structure caused the standard rainflow counting using Miner's rule to estimate fatigue life to be unconservative. Zwerneman and Frank (1988) proposed converting the

complex load-time histories to a single equivalent cycle through the use of a damage index. However, their study indicated that further work was needed to define the damage caused by individual cycles in a variable amplitude load-time history.

Other research has been conducted to evaluate in-service loads of transportation structures. Azzam and Menzemer (2006) evaluated the behavior of welded aluminum light pole support details, Saleem et al. (2012) evaluated an aluminum bridge deck system, and Coughlin and Walbridge (2012) conducted fatigue testing and analysis of aluminum welds under in-service highway bridge loading conditions. These three studies evaluated the components using constant stress amplitude experiments but did not consider an increasing amplitude strain controlled protocol (i.e., Rushing et al. 2016) that could be used to represent subgrade deformation underneath a structure, such as the condition experienced by a mat joint subjected to aircraft loading.

4.4.4 Recent work on AM2 performance prediction

Until recently, all of the full-scale test section data used to develop AM2 predictions were gathered from experiments with mats placed over soils with CBRs from 3 to 10 percent. However, information from users of the matting systems confirmed that the majority of installations over the past 15 years have been over soils with much higher CBR values. As such, more study was needed to predict performance at higher CBRs.

To fill this data gap required to improve the predictability of airfield mat performance, a comprehensive accelerated testing program was initiated in 2005 and continued through 2012. The objective of this program was to evaluate the performance of AM2 over semi-prepared soil surfaces with CBRs of 6, 10, 15, 25, and 100 percent to determine its ability to carry modern aircraft. Details of each of these studies are provided in ERDC technical reports (Rushing and Tingle 2007; Rushing et al. 2008; Rushing and Mason 2008; Garcia et al. 2014a; Garcia et al. 2014b).

AM2 performance was evaluated in full-scale test sections under simulated single-wheel gear F-15E and six-wheel gear C-17 aircraft loads (with the exception of the CBR of 100 percent not being tested with the C-17). The F-15E was represented by a single-wheel tricycle gear loaded to 156.7 kN (35,235 lb) with a tire pressure of 2.24 MPa (325 psi) over a loading width of 22.9 cm (9 in.). The C-17 was represented by a full six-wheel gear loaded

to 1,199 kN (269,560 lb) with a tire pressure of 0.98 MPa (142 psi) with each loading wheel width of 45.7 cm (18 in.). These two aircraft were chosen because they represent loading extremes, i.e., F-15E has high tire pressure and a relatively small footprint (causes severe surface damage), and C-17 has a high maximum gross weight over six-wheels (causes rapid subgrade deformation due to the size and depth of the stress concentration in the foundation soil).

Rushing and Howard (2015) presented a relationship to predict the rate of subgrade deformation based on the F-15E single-wheel loading data. Rushing et al. (2016) further analyzed the single-wheel data set to develop a method to predict the fatigue performance of AM2 and developed a laboratory procedure to predict fatigue without requiring the expense of full-scale experimentation. While the results of these efforts showed considerable improvements to the ability to predict AM2 performance for the single-wheel aircraft, the validity of the process for the complex six-wheel C-17 data set was not considered. This paper attempts to evaluate the subgrade deformation, fatigue, and laboratory test procedure for the six-wheel gear of the Boeing C-17 aircraft as there is a gap in literature in this area.

4.5 AM2 matting

The current matting system predominantly used by the U.S. military and the subject of the study described in this paper is AM2 matting. The AM2 matting system was designed by the U.S. Navy in the 1960s to support heavy single-wheeled fighter aircraft when placed over graded soils with CBRs as low as 4 percent. AM2 is made from a single hollow-core aluminum alloy (AA) 6061-T6 extrusion and is designed to be assembled in a brickwork pattern for greater stability. Pertinent properties are shown in Table 7 from data provided by Rushing and Howard (2015) and Rushing et al. (2016). AM2 panels are joined along their long edges by hinge-type connections with overlap/underlap connections welded to the short ends. A rectangular locking key slot was designed to accept an aluminum key in the underlap/overlap joint to keep adjacent panel ends from vertical separation. Figure 19 depicts AM2 mat panel bundles and the installation of the system over a semi-prepared surface.

Table 7. Properties of AM2 matting.

Length, cm (ft)	Width, cm (ft)	Height, cm (in.)	Density, kg/m² (lb/ft²)	E_{flex}, Transverse, 1 × 10⁴ MPa (1 × 10⁶ lb/in.²)	E_{flex}, Longitudinal, 1 × 10⁴ MPa (1 × 10⁶ lb/in.²)	Material
355 (12)	61 (2)	3.8 (1.5)	31.7 (6.5)	4.30 (6.23)	1.12 (1.63)	AA 6061-T6

E_{flex} = flexural modulus of elasticity.

Figure 19. AM2 mat panels and installation procedures (a) Bundle of AM2 full panels, (b) Bundle of AM2 half panels, (c) Installation of AM2 full panel in full-scale test section, and (d) Installation of locking bar between AM2 panels.

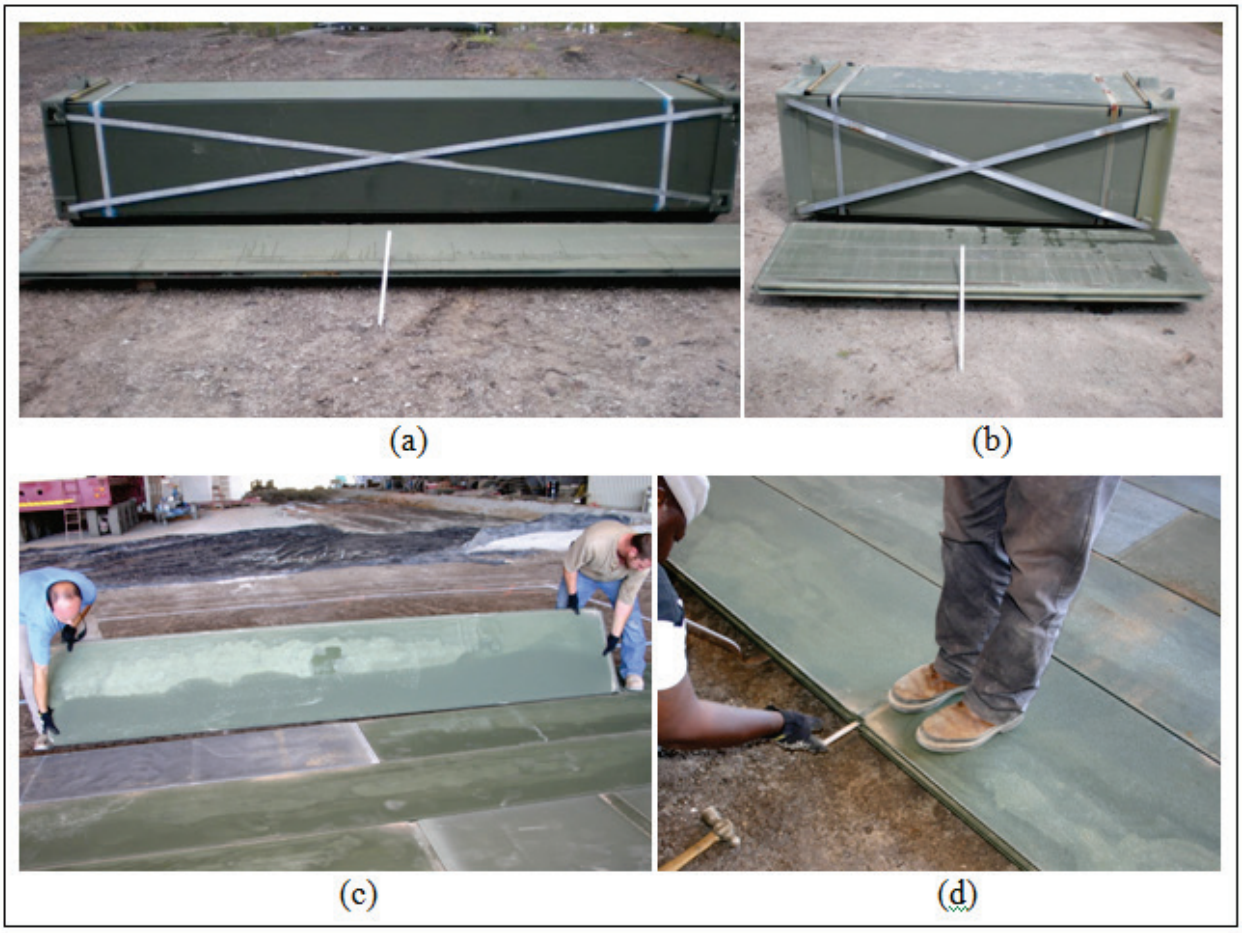

4.6 F-15E performance prediction summary

Analysis of the most recent full-scale data set for the F-15E by Rushing and Howard (2015) resulted in the development of the relationship shown in Equation 12:

$$\delta_s = log_{10}P_n \cdot 1.64 \cdot CBR^{-0.61} \quad (12)$$

where δ_s = the subgrade deformation, in., P_n = the number of passes, and *CBR* is the CBR of the subgrade underneath the structural mat system. This relationship can be used to design the required CBR for a given deformation limit and required number of passes or for evaluation of an existing soil condition to determine the allowable passes based on a deformation limit.

Rushing et al. (2016) derived Equations 13 and 14

$$\frac{CBR}{N_{f-1}} = 6.1\ x\ 10^{-3} \tag{13}$$

$$\frac{CBR}{N_{f-4}} = 4.3\ x\ 10^{-3} \tag{14}$$

to predict low-cycle fatigue failure on the mat under F-15E loads, where *CBR* = the CBR of the subgrade, N_{f-1} = number of F-15E aircraft passes causing the first panel failure in the field experiments, and N_{f-4} = number of F-15E aircraft passes causing system failure in the field experiments. The equations can be rearranged and solved for CBR for use as a design tool to determine the minimum CBR required to meet a mission requirement in terms of passes to the first panel fatigue failure, Equation 13, or overall system failure, Equation 14. The first panel failure, Equation 13, was determined as the number of aircraft passes required to cause the first panel to fail under the applied aircraft loading. System failure was defined as the number of aircraft passes required to fail 10 percent of the panels receiving the aircraft loading and was based on the maximum allowable maintenance requirement by the system users. Conversely, these equations can be used to determine the number of allowable passes based on the CBR of the existing foundation subgrade.

To predict the overall performance of AM2 under F-15E loading, δ_s and N_f were evaluated to determine the controlling condition. For example, if a user required 3,000 F-15E passes (P_n = 3,000) and wanted to know the CBR required to prevent 3.18 cm (1.25 in.) of deformation (δ_s = 3.18 cm [1.25 in.]) or system failure (N_{f-4}), Equation 12 can be solved for *CBR* such that *CBR* = 12 percent, and Equation 14 can be solved where *CBR* = 13 percent; therefore, the relationships predict that fatigue controls, and a minimum CBR of 13 percent is required. For additional information,

Equation 13 can be solved for *CBR* = 18.3 percent or rounded up to 19 percent to give a high level of confidence that no fatigue failures will occur and little or no major maintenance will be required. One can then backcalculate δ_s using Equation 12 with *P* = 3,000 and *CBR* = 19 percent and find that the relationships predict a subgrade deformation of 2.41 cm (0.95 in.) after 3,000 passes. The result is a safety factor of about 1.3 for subgrade deformation if one chooses to use the more conservative fatigue damage equation. This example shows that the choice of Equations 13 or 14 may cause a meaningful effect on the subgrade strength requirement. The level of construction effort required to increase from a CBR of 13 to 19 percent may be costly in terms of time, equipment, and/or materials and should be considered carefully by project or mission planners.

The data analyses represented in the previous paragraphs for the F-15E result in a practical method to predict performance; however, the relationships for the complex behaviors of the C-17 remain unknown. The following sections describe the process for the development of C-17 predictions and a detailed discussion of the results.

4.7 Full-scale test section

The full-scale evaluation of AM2 under simulated Boeing C-17 aircraft traffic was performed by the ERDC under the shelter of a pavement test facility in Vicksburg. The C-17 simulator is shown in Figure 20. The six-wheel main gear was loaded to 1199 kN (269,560 lbf) with a tire pressure of 0.98 MPa (142 psi) with each loading wheel width of 45.7 cm (18 in.). The drive axle weight was 171.26 kN (38,500 lb) with 29.5 by 29 in. tires inflated to 0.21 MPa (30 psi). Since the drive axle represented only 14 percent of the load of the main gear and the tire pressure of the drive wheels was 80 percent lower, the loading effects of the drive vehicle were considered negligible.

Figure 20. AM2 matting panels trafficked by C-17 aircraft simulator in full-scale test section.

Controlled subgrades were constructed to CBRs of 6, 10, 15, and 25 percent as described in Figure 21, and the AM2 matting system was placed directly on the prepared surface as shown in Figure 19. A typical cross section of the constructed test section consisted of 0.91 m (3 ft) of subgrade material processed, placed, and compacted in 15.24-cm (6-in.) lifts over a silt foundation with a CBR of approximately 15 to 20 percent. The CBR of each lift was verified by conducting field CBR tests according to U.S. Army Corps of Engineers (1995) (*Handbook for Concrete and Cement: Standard Test Method for Determining the CBR of Soils*). Simulated C-17 traffic was applied by driving the simulator back and forth over the 12.2-m- (40-ft-) long test section using the wander pattern shown in Figure 22a where the lanes, numbers of passes per lane required to complete a single pattern, and percent traffic distribution per lane are shown for the center tire column in the six-wheel gear configuration (reference point in Figure 22b). When all the tires in the gear were considered, this pattern resulted in traffic application over an approximately 5.5-m- (18-ft-) wide area of matting. Traditional survey methods were used to measure deformation during traffic on the mat surface. Subgrade deformation was monitored by applying a load to the mat surface to push it downward and contact the soil surface once deformation began to occur. Deformation measurements were taken along the traffic centerline and at 15.24 cm (6 in.) intervals for 5.49 m (18 ft) on either side of the centerline. Maximum deformations were generally recorded along the centerline. Fatigue damage was monitored through visual inspection of the mat surface. Additional details of the full-scale tests, test section construction, deformation data, and mat breakage are provided in ERDC technical reports (Rushing and Tingle 2007; Rushing et al. 2008; Rushing and Mason 2008; Garcia et al. 2014a).

Figure 21. Full-scale test section construction sequence (a) Excavating test area in covered pavement test facility, (b) Lining pit with plastic to prevent moisture migration, (c) Mixing soil to achieve uniform moisture, (d) Adding water to adjust moisture content, (e) Compacting processed and installed subgrade material, and (f) Performing field CBR tests to ensure desired value was achieved.

4.8 Subgrade deformation prediction for the C-17

The subgrade deformation (δ_s) data collected from the full-scale AM2 mat evaluation were consolidated and analyzed in an attempt to develop a relationship to predict δ_s when subjected to C-17 loadings. Following the procedure described by Rushing and Howard (2015) for the F 15E, δ_s was plotted as a function of the pass number for each of the CBR tests conducted as shown in Figure 23a. The δ_s values used in the analysis were

Figure 22. C-17 traffic distribution in full-scale test sections (a) Traffic distribution pattern in full-scale test section and (b) C-17 main gear configuration.

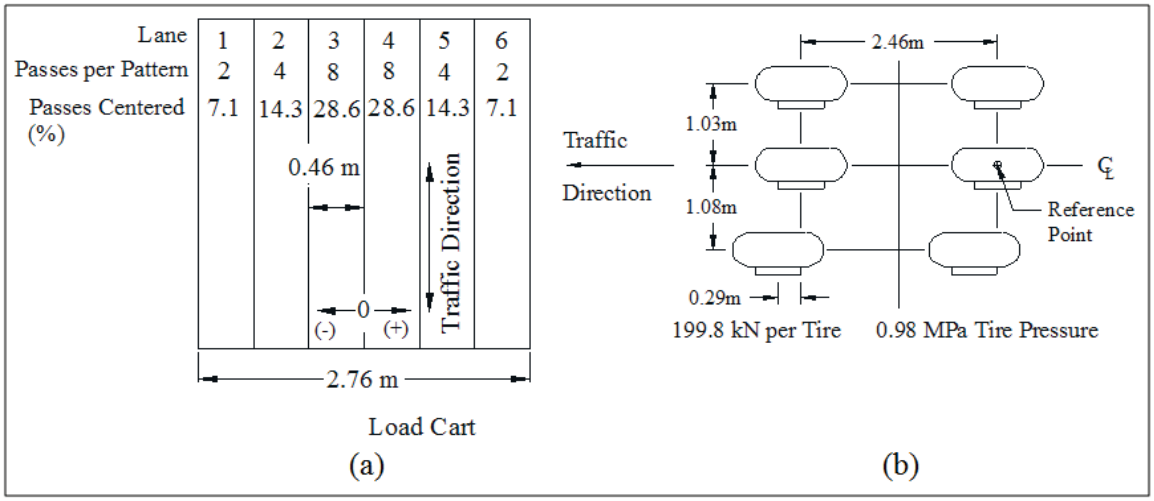

measured using a loaded deflection technique that attempted to load the mat surface enough to contact the subgrade underneath without inducing elastic deformation in the subgrade. Since the matting system was elastic, measurements taken on the unloaded mat surface were not representative of the actual subgrade deformation. Next, logarithmic functions were fit to the δ_s data as shown in Figure 23b. Like the F-15E, the C-17 rut formation is inherently a logarithmic function, where the δ_s increases rapidly during the initial passes and then slows considerably as passes continue to be applied. Since zero passes should result in δ_s = 0, the trends were forced through the origin by taking the $\log_{10}$ of each of the recorded pass numbers so that a 0 value could be manually included in the analysis ($\log_{10}$ of 0 = -∞) with resulting representative equations and their R^2 values displayed in Figure 23c (R^2 values with a forced intercept are for relative comparison only). Since the trends were reasonable predictors of the measured deformations from the full-scale experiments, the analysis was continued. The resulting equations for each respective CBR value were solved for δ_s for 10, 50, 100, 500, 1,000, and 5,000 passes as shown in Figure 24a. For each pass number, an exponential trend was fit to the δ_s predicted for the 6, 10, 15, and 25 percent CBR values. The results showed the trend lines closely matched the predicted values with R^2 values of nearly 0.97. Figure 24a was further simplified into a set of design curves as shown in Figure 24b and resulted in a single three variable equation that closely predicts subgrade deformation for any combination of CBR, number of passes, and δ_s as shown in Equation 15.

$$\delta_s = log_{10}P \cdot 1.92 \cdot CBR^{-0.467} \ (R^2 = 0.97) \quad (15)$$

Figure 23. Full-scale C-17 results for δ_s.

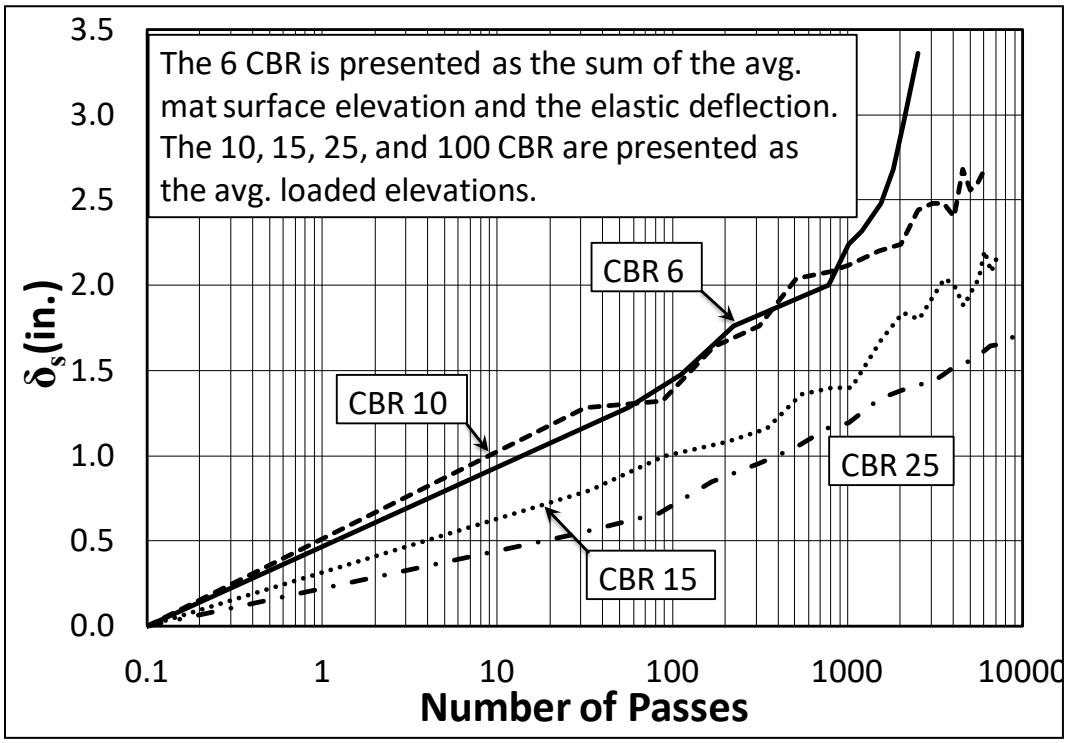

(a)

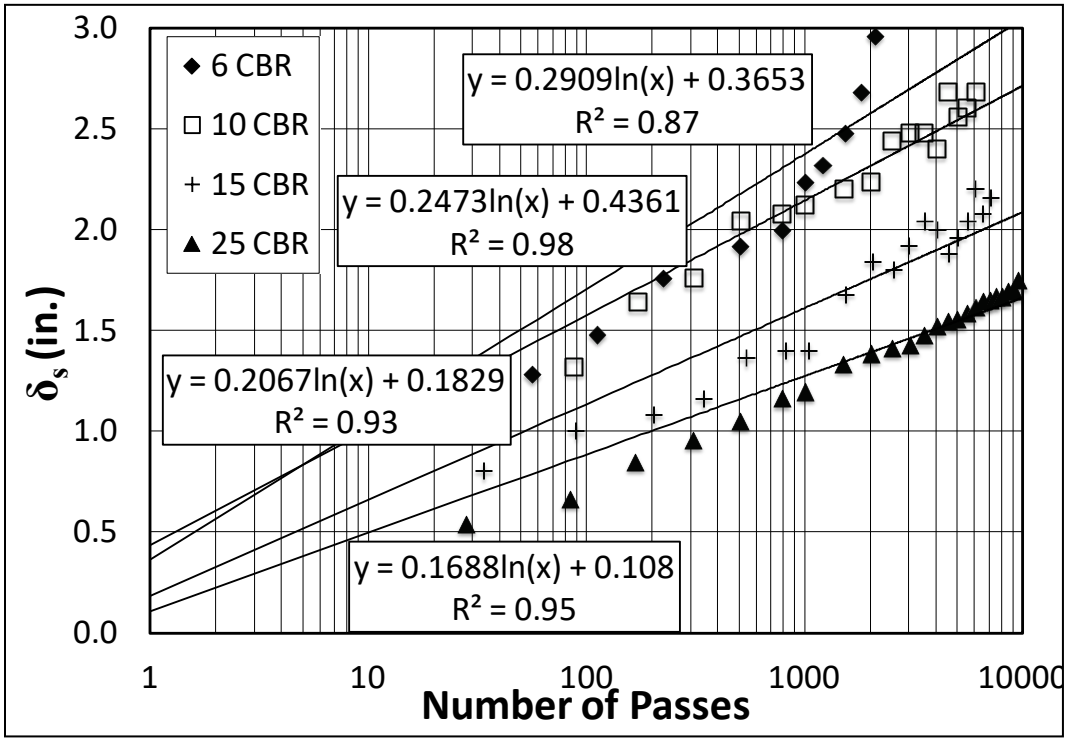

(b)

Figure 23 (continued) (a) δ_s measured for four subgrade CBRs, (b) δ_s best fit predictions, and (c) δ_s predictions with the origin forced through zero.

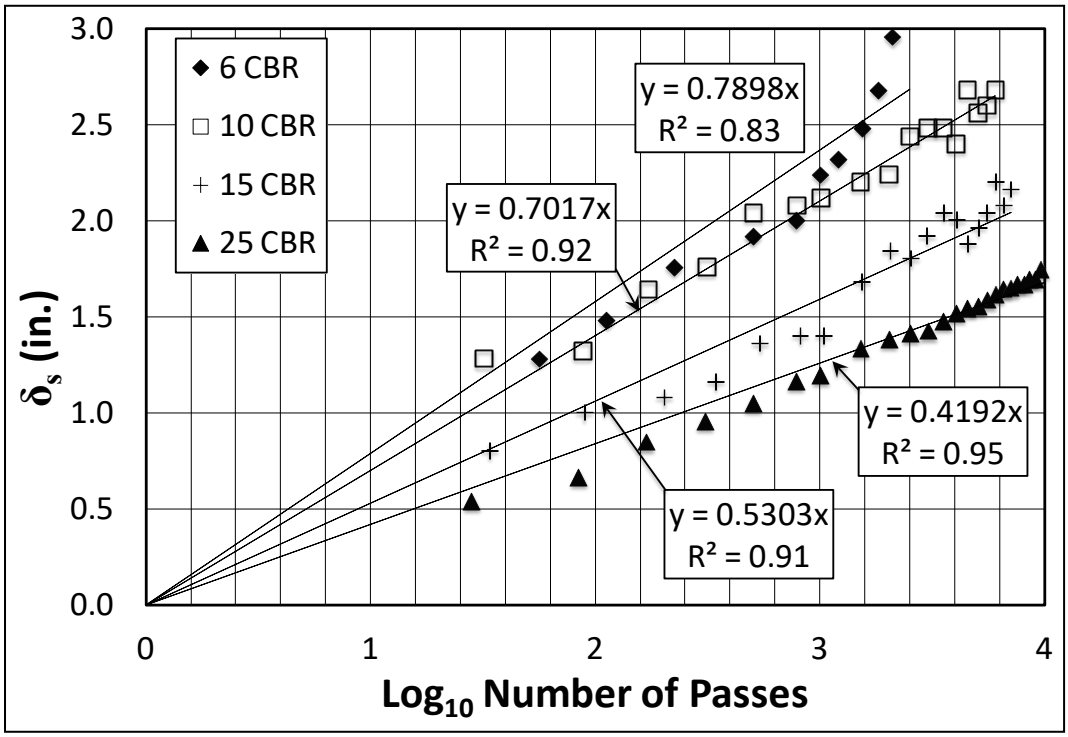

(c)

The term pass to coverage ratio, shown in Figure 24, describes the traffic distribution and is defined as the number of times a loaded wheel crosses a single point in the center traffic lane of the test section. A *pass* is defined as a single crossing of the test section by the test vehicle (either forwards or backwards). The pass-to-*coverage* ratio is the inverse of the sum of probabilities that an aircraft tire will cross a given point on the mat surface during a *pass*. The *pass* to *coverage* ratio for the C-17 main gear along the traffic centerline was determined to be 1.12 for this experiment.

Using the same example as described for the F-15E model, if the user wanted to determine the CBR required to achieve 3,000 passes of a C-17 aircraft while limiting δ_s to 3.18 cm (1.25 in.), Equation 15 can be solved such that *CBR* = 36 percent. In comparison to *CBR* = 12 percent using the same constraints for the F-15E, the prediction equation correctly shows that the C-17 causes noticeably more subgrade deformation for the same number of passes; therefore, the subgrade must be considerably stronger to achieve the same amount of deformation.

Figure 24. C-17 δ_s prediction (a) δ_s predictions for a given number of passes and CBR and (b) δ_s design curves.

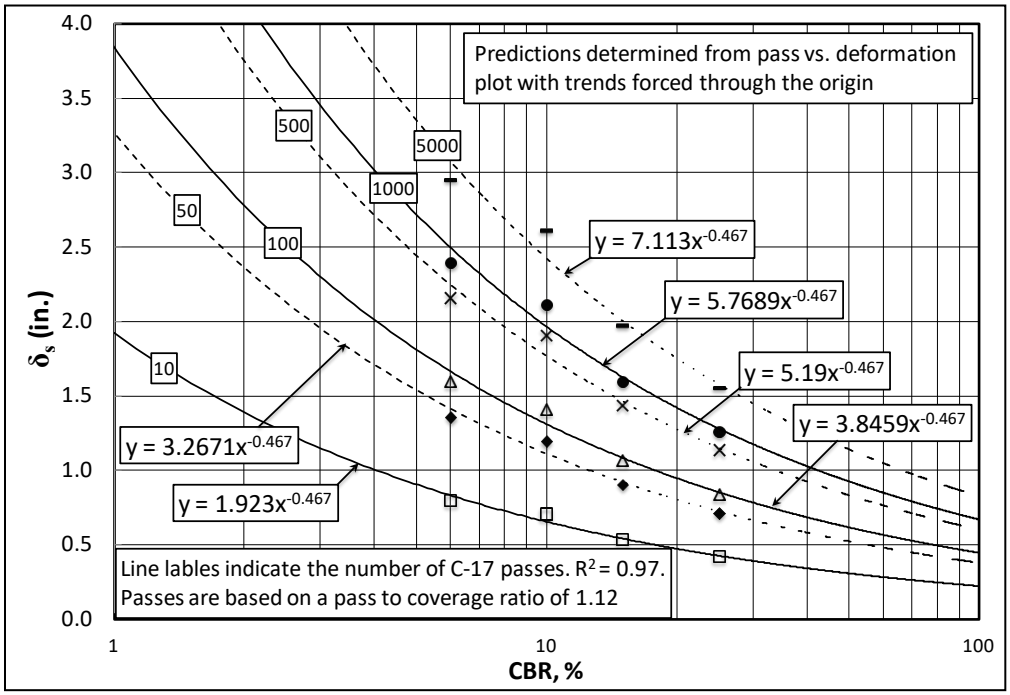

(a)

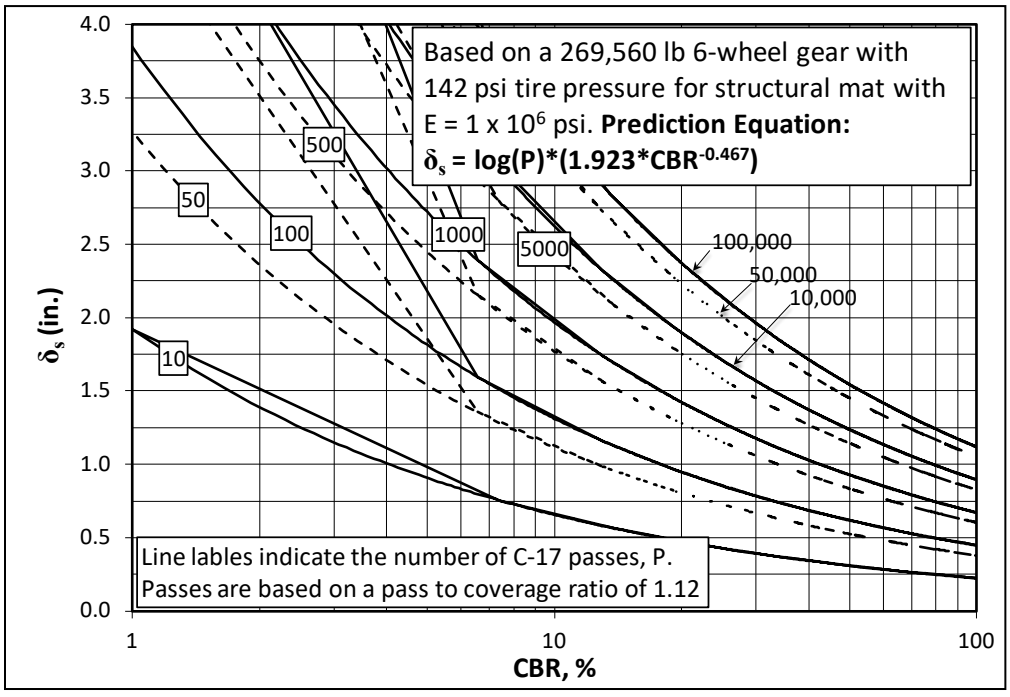

(b)

4.9 Low-cycle fatigue failure prediction for the C-17

In addition to the subgrade deformation prediction, observations of mat low-cycle fatigue damage were analyzed in an attempt to develop a method to predict fatigue behavior. The same process described by Rushing et al. (2016) was followed to develop a low-cycle fatigue failure (mat breakage) relationship as a function of the subgrade CBR and the number of C-17 passes. The AM2 panels were inspected for damage at prescribed data collection intervals throughout trafficking, and any noticeable mat damage was recorded. Trafficking was continued until a minimum of seven panels had failed, representing 10 percent of the trafficked area. The 10 percent failure criterion was set by the project sponsor to represent a reasonable amount of maintenance that could be sustained within an AM2 mat expanse. Any additional damage was determined to be excessive and therefore was not allowed. As described in Rushing et al. (2016), the majority of the fatigue failures were found to occur in the upper underlap rail of the 2-ft end connector of the AM2 joint. These failures were determined to occur by stress concentrations located at region 1 in Figure 25b when the panel was loaded on the underlap side of the joint and the locking bar used to prevent panel separation induced bending of the upper underlap rail. With successive passes, this stress concentration allowed crack incubation and small crack growth as shown in Figure 26a. Eventually, the cracks propagated through the upper underlap rail and caused complete separation from the panel as shown in Figure 26b, resulting in panel failures.

Even though the damages were similar, there were noticeable differences in the fatigue behavior from the F-15E and C-17 evaluations. Since the F-15E has a small footprint and a high tire pressure, fatigue damage to the mat panels was easily observed. However, the large footprint of the massive six-wheel C-17 gear depressed a large area of the mat downward into the subgrade and made damage within the 60.1-cm- (24-in.-) panel ends difficult to observe. As the strength of the subgrade was increased, observation of failures became even more difficult. Therefore, first panel failures were identifiable only for the experiments over CBRs of 6 and 10 percent.

Figure 25. Laboratory test fixture and boundary conditions (a) Laboratory test boundary conditions, (b) Areas of stress concentration in laboratory experiment (not to scale), and (c) Photo of experimental laboratory test fixture.

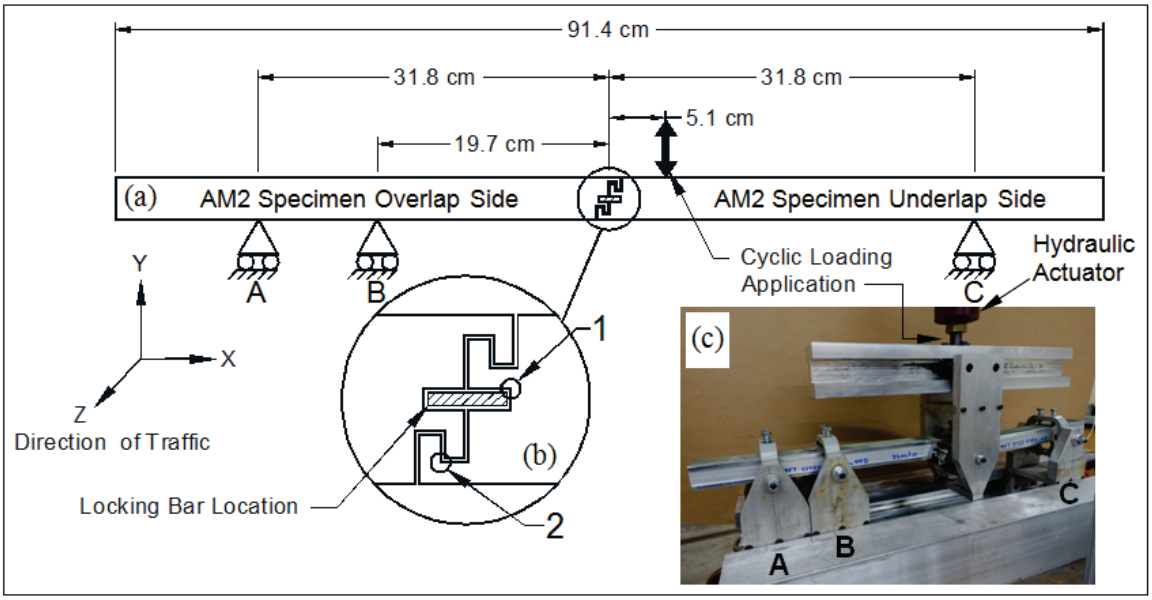

Figure 26. Typical AM2 fatigue failures (a) Close-up of crack in upper underlap rail at critical stress location from load transferred through the locking bar and (b) Upper underlap rail completely separated from AM2 panel during a full-scale traffic experiment.

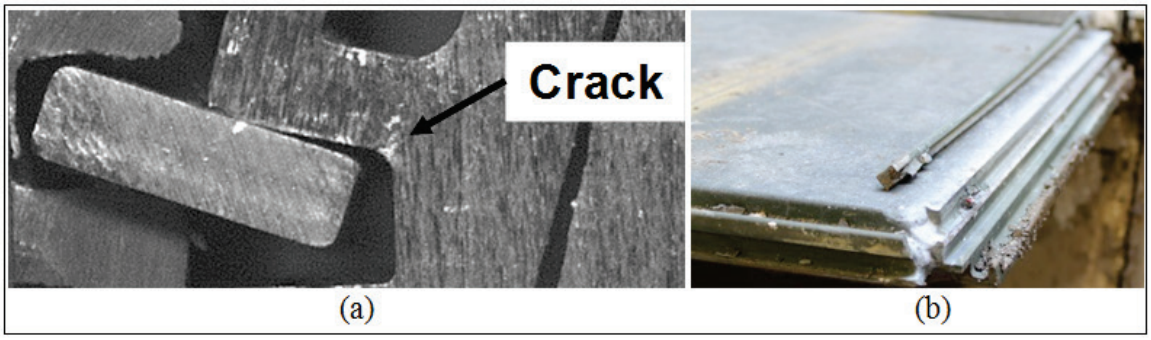

Because of this effect, only the system failures (failure of 10 percent of the trafficked area) were analyzed for the C-17 experiments. Furthermore, after 10,000 simulated aircraft passes over a CBR of 25 percent, no panel damage had occurred. Traffic was stopped to prevent excessive maintenance cost and excessive wear on the trafficking vehicle.

Fatigue failures from the full-scale traffic experiments are shown in Figure 27. If trafficking had been continued to failure for the CBR of 25 percent, the trend shown in Figure 27 would likely have been further

strengthened. The results indicate that system failure of the C-17 can be reasonably predicted by Equation 16,

$$CBR = 0.1237 * {N_f}^{0.5452} (R^2 = 0.84) \quad (16)$$

where CBR = CBR of the underlying soil and N_f = number of allowable C-17 passes prior to system failure.

Continuing the same example as shown for the F-15E earlier in this paper to predict the CBR required for 3,000 aircraft passes with a δ_s limit of 3.18 cm (1.25 in.) and system failure, Equation 16 was solved for CBR = 10 percent. Since the CBR required to prevent the subgrade deformation was CBR = 36 percent, subgrade deformation controls in this case.

Figure 27. Mat breakage fatigue results for system failures.

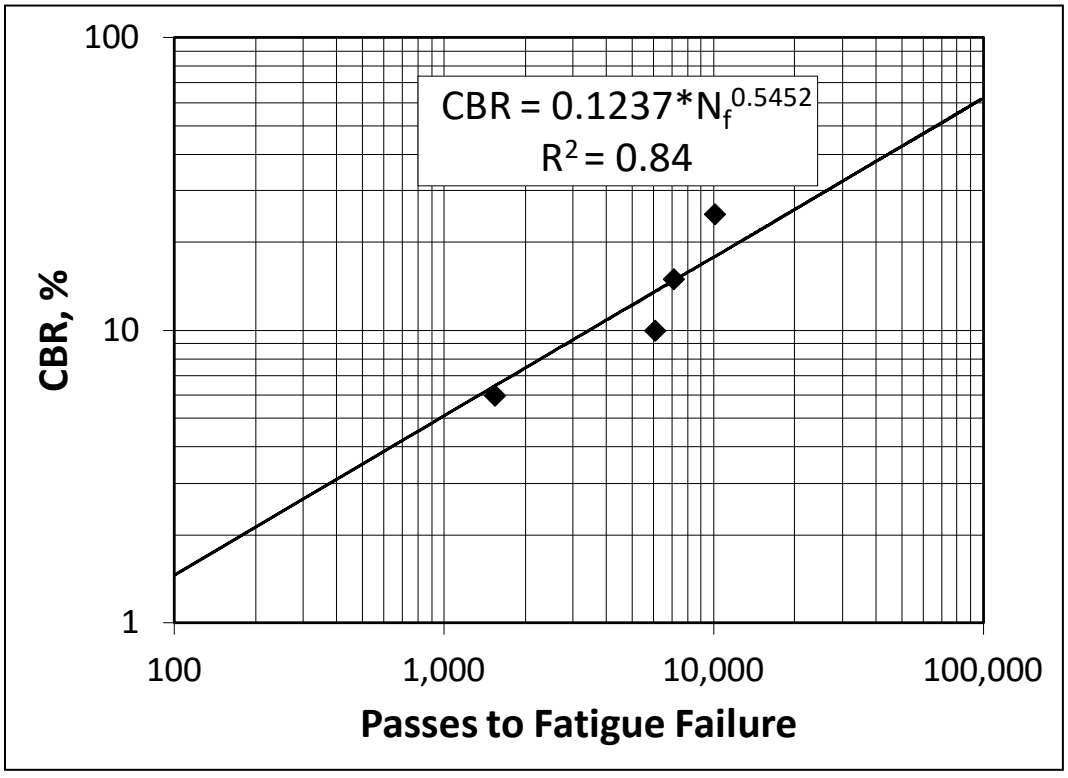

4.10 Laboratory fatigue experiments

Researchers were aware that the low-cycle fatigue behavior of the AM2 mat system was directly related to the subgrade deformation caused by repetitive load applications. In an attempt to couple these two behaviors together in a laboratory environment, Rushing et al. (2016) used the F-15E

δ_s prediction equation and knowledge of low-cycle fatigue behavior of the AM2 matting system to develop a novel laboratory fixture and procedure to predict the number of cycles to fatigue failure for any subgrade CBR of interest using an increasing amplitude displacement controlled test. The purpose of this development was to enable researchers to test variations of the AM2 joint design in the laboratory to avoid full-scale experiment expenses. A detailed description of the experimental fixture and the methods and reasoning that led to its design is described by Rushing et al. (2016), and the final laboratory test configuration is shown in Figure 25. The procedures used to determine the location of the fixtures constraints and the increasing amplitude displacement function were first repeated in this study to determine if the methods used to predict fatigue failure of the AM2 joint under F-15E loading conditions can be repeated with success for the C-17 loading.

The test fixture described in Figure 25 was designed to accept 5.08-cm- (2-in.-) wide AM2 specimens cut across the 61-cm (24-in.) welded fatigue critical joint that were 45.7 cm (18 in.) long on each side of the joint centerline. Once the joint was assembled and a locking bar was inserted to prevent vertical separation of the joint, the entire specimen was approximately 91.4 cm (36 in.) long. Each constraint (locations labeled A, B, and C in Figure 25a) and loading location was constructed from a section of a box beam, and set screws were tapped into the top and bottom to sandwich the specimen and hold it in place. Pinned connections were used to allow the box beam section to rotate freely, and a system of tracks and bearings was designed to allow for freedom of horizontal movement. The underlap side of the AM2 joint was constrained only in the vertical direction 31.8 cm (12.5 in.) from the joint centerline as shown by location C in Figure 25a.

An increasing amplitude cyclic displacement function was applied 5.1 cm (2 in.) from the underlap end of the joint using one of the previously described box beams so that a downward displacement could be applied and the specimen could be returned to its pre-loaded vertical position. The overlap side of the joint was fixtured as a cantilever beam, as shown in Figure 25a, and was constrained only in the vertical (Y) direction (pinned rollers) at the two locations (labeled A and B in Figure 25a). The first and second constraint locations were determined through a calibration procedure described later in this section.

The increasing amplitude displacement function for the C-17 used in the laboratory experiment was determined for CBRs of 6, 10, 15, and 25 percent by calculating δ_s from Equation 15 for P_n = 0 to 10,000 as shown in the primary axis in Figure 28. For each of the CBR values of interest, δ_s values were multiplied by a slope correction factor, S_c, and programmed into an MTS Systems Corporation hydraulic actuator control and data acquisition system. In this case, $S_c = \frac{d_{lab}}{D_{field}}$ where D_{field} is the maximum allowable downward movement of the joint location during full-scale loading and d_{lab} is the maximum vertical displacement in the laboratory required to cause contact of the lower tabs at the location shown in Figure 25b. Once contact occurred in this location, the specimen would rotate further than field constraints allowed, and the joint would fail in region 2 in Figure 25b. This condition was not observed in the full-scale experiments.

Figure 28. Field and laboratory calculated displacements for CBRs of 6, 10, 15, and 25 percent.

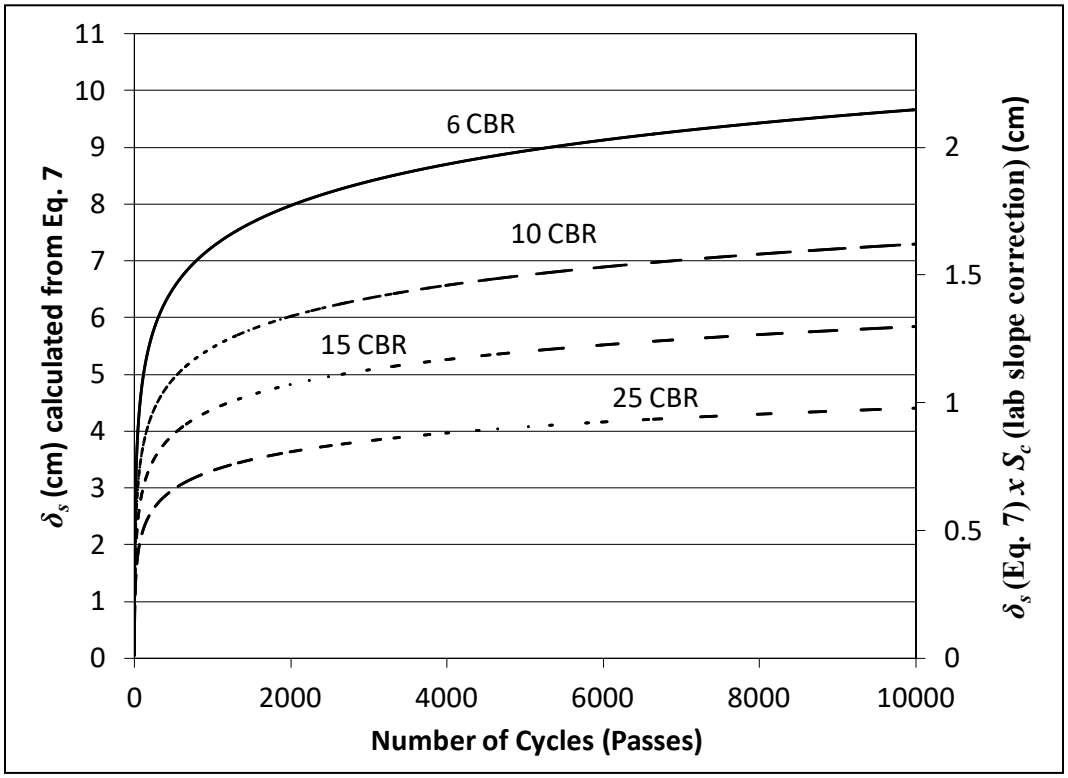

During field experiments, the width of the subgrade deformation, W_{field}, measured approximately 2.74 m (9 ft) as shown in Figure 29 (note the large disparity between F-15E and C-17 rut profiles) since the traffic was

applied over a 5.48-m- (18-ft-) wide area, and 7.62 cm (3.0 in.) of downward movement, D_{field}, was required to rotate the end joints far enough for the area in region 2 in Figure 25b to be affected. Because the full-scale tests were concluded at or shortly after 7.62 cm (3.0 in.) of subgrade deformation had developed, failures in this region were not observed. Since the maximum allowable vertical displacement to cause contact in region 2 in Figure 25b in the lab measured 1.59 cm (0.625 in.), d_{lab}, the w_{lab} required to develop the same angle of rotation in the joint was determined by solving the ratio in Equation 17

$$\frac{D_{field}}{W_{field}} = \frac{d_{lab}}{w_{lab}} \tag{17}$$

where w_{lab} = 57.2 cm (22.5 in.). To maintain a consistent rotational degree in the laboratory experiments, the programmed displacements calculated using Equation 15 were multiplied by $S_c = \frac{d_{lab}}{D_{field}}$ = 0.21 as shown in the secondary y-axis in Figure 28.

Figure 29. Comparison of C-17 and F-15E subgrade deformation at failure used for laboratory slope calculations.

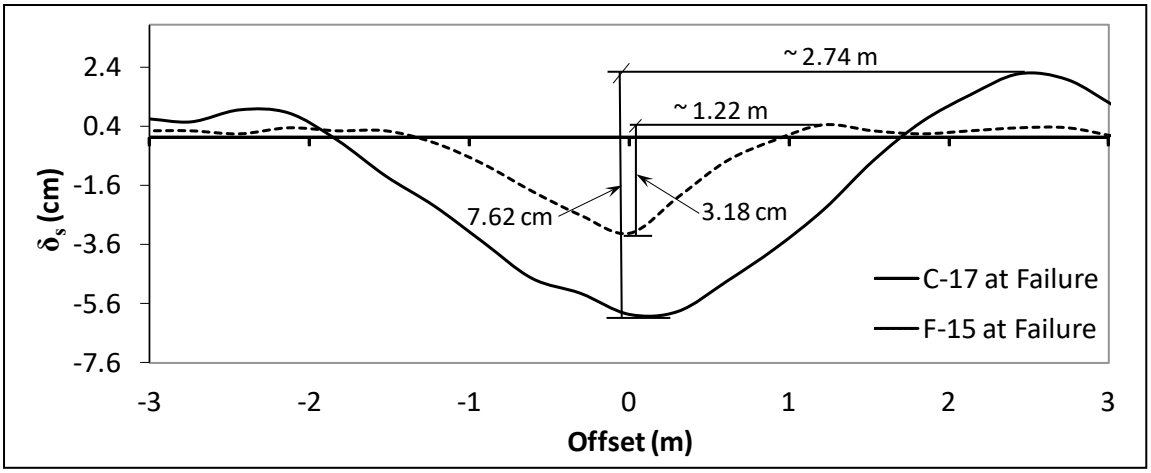

The displacements for this experiment were applied at a rate of 0.5 Hz and resulted in a loading range from 0 to 22 kN (5,000 lbf), and the data acquisition rate was set at 51.2 Hz. Time, load, and displacement were recorded continuously throughout the experiments. Calibration of the test fixture was achieved by moving the location of the interior constraint (labeled B and shown in Figure 25a) on the cantilevered side of the joint until approximately 16.9 kN (3,800 lbf) of vertical load was required to displace the center of the joint 1.59 cm (0.625 in.) downward. The 16.9-kN

(3,800-lbf) load was calculated by taking the load applied by one of the six C-17 wheels, 1,199 kN (269,560 lbf)/6 wheels = 200 kN (44,927 lbf), and dividing by the length of the joint (60.1 cm [24 in.]). This resulted in approximately 3.33 kN per cm (1,872 lbf per in.) of joint. Since the laboratory specimen was 5.08 cm (2 in.) wide, the approximate loading at the maximum allowable joint rotation was calculated as 8.33 kN (1,872 lb) × 5.08 cm (2 in.) = 16.89 kN (3,744 lbf) or approximately 16.9 kN (3,800 lbf).

New test specimens were used for calibration. A specimen was inserted into the test fixture with the interior constraint on the cantilevered side of the joint at location B in Figure 25a positioned 19.7 cm (7.75 in.) from the centerline of the joint. A vertical load was applied until the displacement measured 1.59 cm (0.625 in.), and the load was recorded. This initial position resulted in an applied load of approximately 17.4 kN (3,900 lbf). Since the load required to achieve the desired displacement was slightly higher than required, the position of the interior constraint at location B in Figure 25a was adjusted to 20.32 cm (8.0 in.), and the load was reduced to approximately 15.12 kN (3,400 lbf) at 1.59 cm (0.625 in.) displacement. Researchers determined that some of the load from the C-17 was carried by the longitudinal joints in the mat since the footprint of the tire spanned about 55.9 cm (22 in.) of the mat in comparison to only about 30.5 cm (12 in.) for the F-15E. Therefore, the experiments were conducted with the constraint in location B in Figure 25 at 20.32 cm (8.0 in.) because the reduced load was more appropriate to approximate the actual load that was transferred to through the 61-cm (24-in.) panel end connector of the mat.

Preliminary laboratory test configurations used to develop the calibration procedure showed that if the applied vertical load exceeded field conditions prior to achieving a displacement of 1.59 cm (0.625 in.), the specimen would fail prematurely when compared to full-scale observations. If too little load was applied prior to a displacement of 1.59 cm (0.625 in.), the specimen would rotate further than field constraints allowed, and the joint would fail in region 2 in Figure 25b. This condition was not observed in full-scale experiments.

The calibration method was chosen to best represent the conditions experienced by the joint from the full-scale experimentation and ensured the specimen failed in the fatigue critical zone, shown as region 1 in

Figure 25b, that was observed in the majority of failures in the full-scale experiments. The increasing amplitude displacement function calculated using Equation 15 and slope correction factor, S_c, for a CBR of 6 percent was used to calibrate the test fixture, and the three constraint locations (A, B, and C shown in Figure 25) were repeated for all the initial experiments for CBRs of 6, 10, 15, and 25 percent.

4.11 Results of laboratory experiments

Laboratory experiment results in terms of number of cycles to failure are shown in Figure 30 for the initial calibration as described above for simulated CBR values of 6, 10, 15, and 25 percent (16 total tests) and for a re-calibrated sample set of five replicates for a CBR of 15 percent to be discussed in the following section. The initial sample set includes five replicates tested under simulated CBRs of 6, 10, and 15 percent and one at 25 percent to match those conducted by Rushing et al. (2016) for the F-15E loading condition. This study focused on the predictability of the lower range of CBR values because full-scale experimental results indicated that the failure mechanism shifted to the core of the panel as the subgrade deformation was meaningfully decreased for higher CBRs.

Figure 30. Results of laboratory fatigue failures.

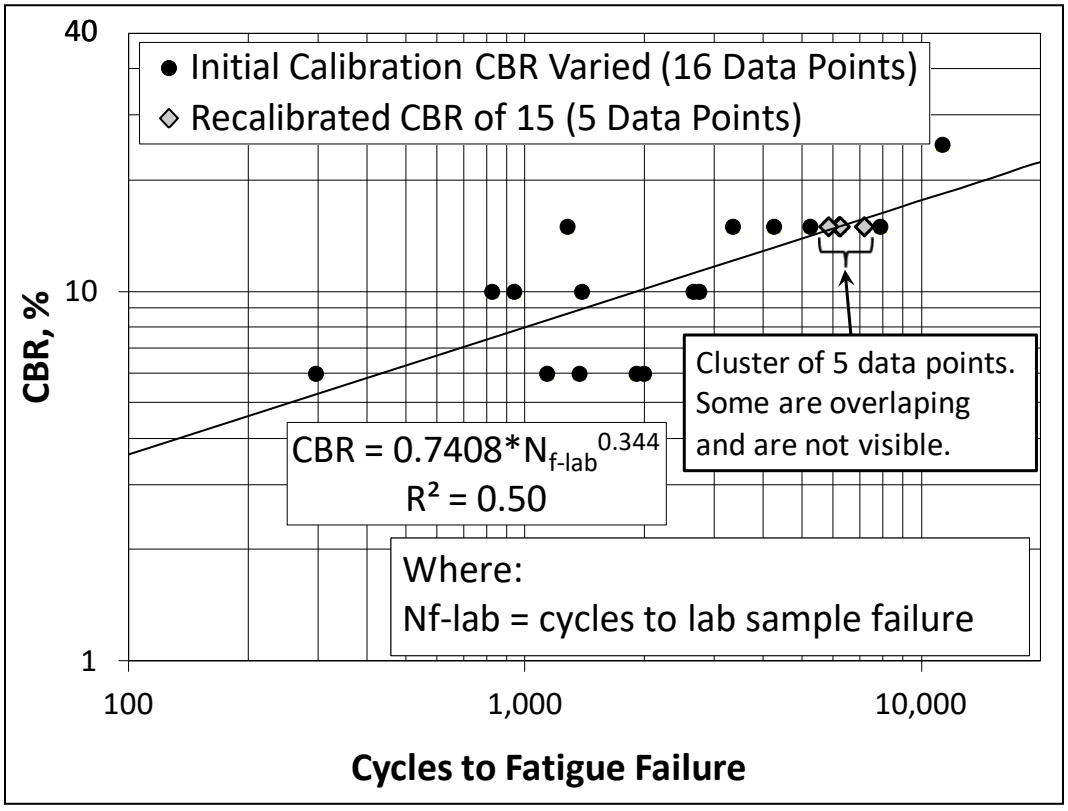

Considerable scatter of the data can be observed in Figure 30. This scatter is thought to be the result of asymmetrical loading across the specimen joint caused by movement of the locking bar in its slot upon unloading during testing, causing the precise point of loading during each successive cycle to be unpredictable. Furthermore, the designed "slack" in the joint and freedom of both vertical and horizontal movement of the test likely led to further changes in the position and magnitude of load concentration throughout the test. However, since the goal of the laboratory test fixture and experimental procedure was to mimic field conditions as closely as possible, this level of movement during the test was expected and is reasonable. From the initial test results in Figure 30, results of Equation 18 represent the data with an R^2 of 0.50, where $N_{f\text{-}lab}$ is the number of cycles required for failure of the joint in the laboratory specimen and *CBR* is the programmed subgrade bearing capacity.

$$\frac{CBR}{N_{f-lab}{}^{0.344}} = 0.74 \quad (18)$$

To reduce the scatter effect in both the full-scale and laboratory experimental data and to strengthen the predictability of failure, the full-scale experimentation data were normalized to account only for loading cycles that occurred on the underlap side of the joint. Because the location of the center of the six-wheel C-17 gear during the full-scale experiments was approximate and complex, the gear shown in Figure 22b was superimposed over each Figure 22a traffic lane to determine the number of damage cycles that were experienced by the joint during completion of a 28-pass traffic pattern. Researchers concluded that 36 damage cycles occurred for every 28 aircraft gear passes (out of 6 wheels × 28 passes = 168 possibilities). The remaining load cycles were determined to primarily load the overlap side of the joint and did not cause meaningful damage. Therefore, the number of cycles required for panel failure, N_f, during the full-scale experiment were multiplied by a damage factor of 1.2857 (or 36/28). The resulting values of N_f for each tested CBR were plotted with the average laboratory experimental values, $N_{f\text{-}lab\text{-}avg}$, to assess predictability, as shown in Figure 31. Power function trendlines were added to each specimen set with their intercepts forced through the origin to compare their ability to predict passes-to-failure. The results show a close match for the CBRs of 6 and 25 percent, but there was still noticeable variability for the CBRs of 10 and 15 percent.

The data provide evidence that the designed laboratory loading procedure and boundary conditions presented herein are representative of the actual conditions that occur in the field for a six-wheel load configuration, although they are not as conclusive as those shown by Rushing et al. (2016) for the single-wheel F-15E loading condition. Using this procedure, users can reasonably estimate the number of cycles required to induce fatigue failure in the AM2 joint without requiring costly full-scale test section construction.

Figure 31. Comparison of full-scale system failure and average failure from laboratory experiments at a given CBR.

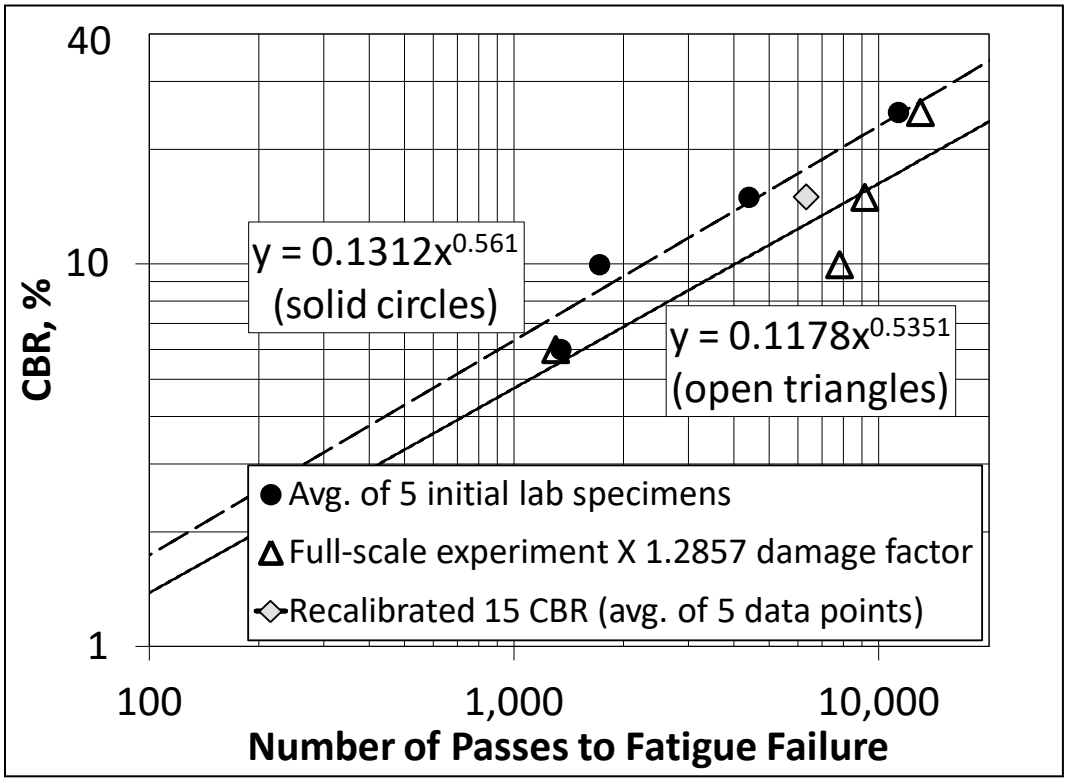

4.12 Discussion of laboratory fatigue test results

Results from the laboratory experiments showed meaningfully more scatter than observed by Rushing et al. (2016) for the single-wheel F-15E loading, thus requiring further analysis in an attempt to determine the cause of the variability, even though the complexity of the C-17's six-wheel gear was expected to be more difficult to mimic in a laboratory procedure. The most significant difference in the two loading configurations, for example, is that in the laboratory experiments a single force is applied over a narrow sample of the mat joint; however, in the field, the six-wheel C-17

main gear applies an array of forces across a relatively large expanse of the mat-surfaced area.

Some of the early failures that occurred using the initial calibration procedure in the laboratory tests were unexpected, and researchers were concerned that the specimens were being overloaded too early during the experiments. Most notably, the induced load may have been greater than the actual full-scale loading conditions. After reviewing the initial test results, five untested specimens remained. To test the hypothesis that specimens might have been overloaded during initial lab tests (in Figure 30), the length of the cantilever on the overlap side of the joint was increased by moving support B in Figure 25a from 20.32 cm (8.0 in.) to 20.96 cm (8.25 in.) to effectively reduce the maximum load accumulated at 1.59 cm (0.625 in.) of displacement from approximately 15.12 kN (3,400 lb) to 12.90 kN (2,900 lb), and five replicates were tested at a CBR of 15 percent. The results of these five replicates are shown in Figure 30 (replicate values are 6,192; 6,196; 6,232; 5,822; and 7,163) and the average of these five tests in relation to field results is shown in Figure 31 (average = 6,321).

Actual measured maximum load accumulations prior to failure reduced on average from about 12.01 kN (2,700 lb) to 10.68 kN (2,400 lb) at failure for the 20.32-cm (8.0-in.) and 20.96-cm (8.25-in.) cantilever lengths, respectively. Changing the length of the cantilever noticeably reduced the scatter in the data; all five specimens failed within a few hundred cycles of each other and, as shown in Figure 31, moved the failure cycles much closer to the observed field value for the CBR of 15 percent. The reduction in loading appeared to be just enough to reduce the tendency of the specimens to fail prematurely, although further testing of additional replicates at other CBR values is needed to make more detailed statements about this hypothesis. Even so, this test showed that it is, in fact, possible to reduce the scatter in the number of cycles to failure using the laboratory procedure presented herein by adjusting the boundary conditions, which may lead to better predictability of field performance.

To further study causes of variability in the number of cycles to failure, cylindrical fatigue coupons were taken from AM2 mat joints to investigate the variability in fatigue failure in the as-extruded AA 6061-T6 material used to manufacture the mats. Following procedures in ASTM E606/

E606M-12, strain-controlled fatigue tests were conducted using five different strain conditions and three or four replicates to assess variability. The results of these experiments are shown in Figure 32. As shown in Figure 32, there is meaningful scatter in the data even during highly controlled, nearly identical tests using the base material. These results indicate that the observed scatter from the laboratory tests of the AM2 joint specimens is not only attributed to variability in the loading and location of the stress concentration, but is also an inherent behavior of the base AA 6061-T6 material. Therefore, the Figure 25 laboratory test data should contain variability as the base material has some variability, which is encouraging for the longer term value of this test.

Figure 32. Results of strain-controlled fatigue experiments of as-extruded AA 6061-T6 from AM2 mat joint section.

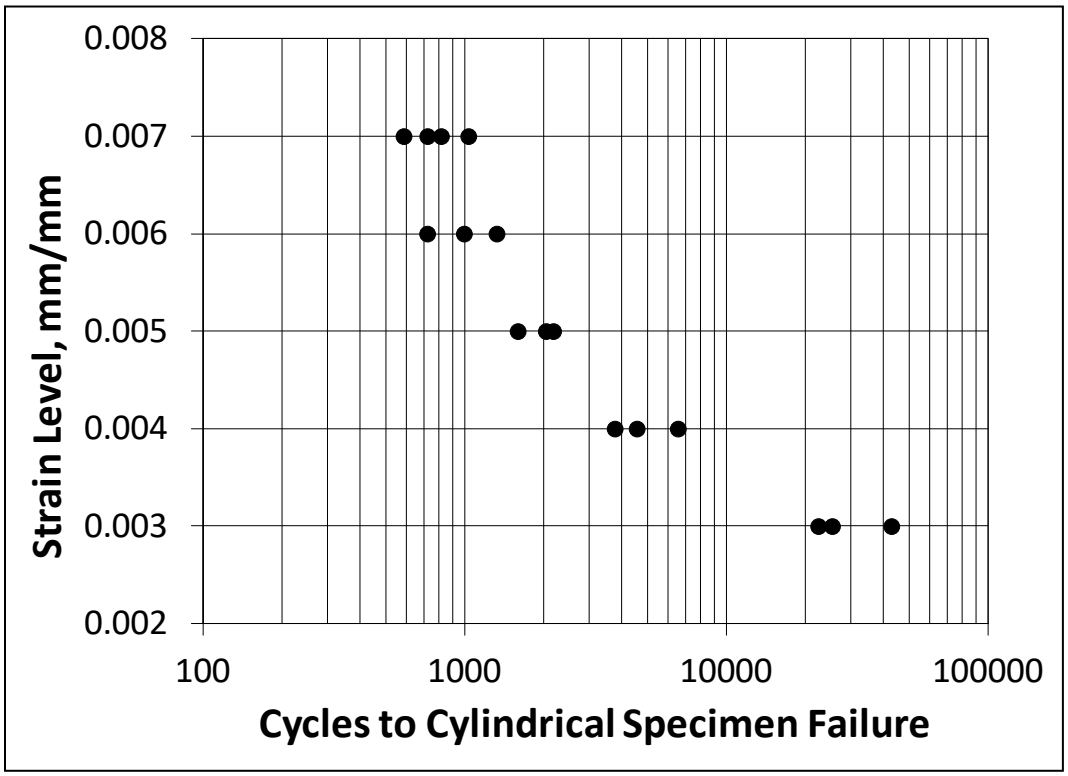

4.13 Conclusions and recommendations

The objectives of this paper were to analyze results from full-scale accelerated tests of AM2 matting subjected to simulated Boeing C-17 aircraft traffic and to develop equations to predict the subgrade deformation and AM2 fatigue damage for any subgrade CBR. Additionally, a novel laboratory experimental test fixture, calibration method, and loading procedure were proposed as a method to evaluate AM2 mat joints under

representative field conditions. These three objectives follow (and build upon) the authors' previous work for a simpler, single-wheel load case using simulated F-15E loads in an attempt to validate the usefulness of the equation and laboratory developmental procedures for the complex six-wheel C-17 aircraft main landing gear. Based on the stated objectives, the following conclusions were drawn.

- The relationship developed in Equation 15 appears to be a reliable predictor of subgrade deformation underneath the AM2 mat system as a function of the number of aircraft passes and subgrade CBR. This proposed relationship is practice-ready and can be used for both design and evaluation of existing conditions.
- Equation 16 was determined to be a reasonable predictor of low-cycle fatigue failure of the AM2 mat system when subjected to C-17 traffic loadings as a function of the subgrade CBR. This equation is also practice-ready and can be used for both design and evaluation.
- Both Equations 15 and 16 must be employed to determine the controlling failure condition (excessive subgrade permanent deformation or inadequate low-cycle fatigue resistance) based on conditions set by the user.
- The laboratory test fixture and the increasing amplitude test procedure described in this paper offer a novel approach to the evaluation of a mat joint by closely representing loading and boundary conditions experienced in field conditions. Although there was meaningful scatter in the data as compared to the results indicated by Rushing et al. (2016) for the F-15E, further adjustment of the calibration procedure may increase the precision of the results. Even with variability, a comparison of the average laboratory results with the full-scale test data showed very good agreement. This approach can be used as a risk-reduction tool when evaluating new mat structural and end connector designs and could also be economical by reducing full-scale testing needs.
- The approach described herein to use predicted soil deformations to derive an increasing amplitude displacement function to evaluate any CBR seems to be a unique approach to low-cycle fatigue failure of a system component of a transportation structure placed directly on a semi-prepared soil surface and subjected to vehicle traffic. A similar approach may be useful to other practitioners interested in testing the effects of a structural system component over a cyclically deformable media if deformation prediction tools are available.

The deformation and fatigue prediction relationships for the Boeing C-17 presented in this paper are part of a larger effort consisting of four major emphasis areas, i.e., (1) development of equations to predict subgrade deformation for F-15E loading as described by Rushing and Howard (2015) and presented herein for the C-17, (2) development of an equation to predict fatigue failure of AM2 as a function of the subgrade CBR for F-15E loading as described by Rushing et al. (2016) and presented herein for the C-17, (3) creation of a design and evaluation framework used to determine the subgrade strength required to support a specified number of aircraft passes or to determine the number of allowable aircraft passes for a given subgrade strength, and (4) development of a laboratory test fixture and procedure to evaluate mat joints to reduce the need for full-scale test sections. Future work is needed to relate these functions to all loading conditions and mat systems other than AM2 to support a broader range of operational conditions.

4.14 Acknowledgements

The full-scale and laboratory experiments and resulting data presented in this chapter were obtained from research conducted at the U.S. Army ERDC, Geotechnical and Structures Laboratory (GSL), Engineering Systems and Materials Division, Airfields and Pavements Branch with funds provided by the U.S. Air Force Civil Engineer Center (AFCEC) and the office of the Assistant Secretary of the Army for Acquisitions, Logistics, and Technology (ASAALT). The sponsors determined the scope of the study but did not assist in data collection, analysis, or writing. The support of AFCEC, ASAALT, and ERDC personnel is gratefully acknowledged. A special thank you goes to Jeb Tingle, Quint Mason, Tim McCaffrey, and Lyan Garcia, of the ERDC GSL, who were instrumental in the successful completion of this research. Permission to publish this work was granted by the Director, Geotechnical and Structures Laboratory.

5 Conclusions and Recommendations

5.1 Conclusions

The overall goal of this report was to provide improved relationships that can be used to predict subgrade deformation underneath an AM2 mat installation and the associated fatigue damage when subjected to F-15E and C-17 traffic. Additionally, a laboratory fixture and procedure were described that can be used to evaluate an AM2 style joint in fatigue and directly relate its performance to in-situ field CBR conditions without requiring the expense of full-scale testing. Throughout this report conclusions were drawn and are summarized below.

- Results from the full-scale tests showed that the relationship currently used to predict mat performance, shown in Equation 1 and based on the CBR design procedure for flexible pavements, greatly overestimates the number of allowable passes for soils with CBRs greater than 10 percent and does not differentiate deformation and fatigue damage.
- The subgrade deformation relationship shown in Equation 3 for the F-15E aircraft is a reasonable predictor of field response for AM2 surfaced airfields. This proposed relationship is practice-ready and can be used for both design and evaluation.
- The relationships shown in Equations 4 and 5 are capable of predicting fatigue failures ($N_{f\text{-}1}$ and $N_{f\text{-}4}$) of AM2 under F-15E loadings for any subgrade support condition. These proposed relationships are practice-ready and can be used for both design and evaluation of AM2 surface airfields.
- The subgrade deformation relationship shown in Equation 15 for the C-17 aircraft appears to be a reliable predictor of field response for an AM2 surfaced airfield. This proposed relationship is practice-ready and can be used for both design and evaluation of existing conditions.
- Equation 16 was determined to be a reasonable predictor of fatigue failure of the AM2 mat system when subjected to C-17 traffic. This equation is also practice-ready and can be used for both design and evaluation.
- The laboratory test fixture and the increasing amplitude test procedure described in Chapters 3 and 4 offer a novel approach to the evaluation of a mat joint by reasonably representing loading and boundary conditions experienced in field conditions. Although there was meaningful scatter in the C-17 data, as compared to the F-15E data, the average

laboratory results showed good agreement with the results of the full-scale experiments. This approach can be used as a risk-reduction tool when evaluating new mat structural and end connector designs and could also be economical by reducing full-scale testing needs.

5.2 Recommendations

The work presented in this report specifically addressed the behavior of an AM2 mat-surfaced airfield subjected to F-15E and C-17 aircraft loadings. Based on lessons learned during the conduct of the research presented in this report, the following recommendations and suggestions for future work are provided:

- The use of the relationships developed in this report for design and evaluation of AM2 surfaced airfield is recommended for practical implementation because it offers improvement over existing methods.
- The full-scale evaluations described in this report utilized new AM2 matting. Because of the system's robust construction and typical installation over CBRs greater than 25 percent (preferred when possible), field failures are not common. Therefore, some airfields may be surfaced with "used" AM2 matting without a recorded usage history. Future work could develop reduction factors to account for some loss in fatigue life when surfacing airfields with "used" AM2.
- Logistical considerations often lead to more half panels of AM2 matting at an installation location than required to create a brickwork pattern. Therefore, alternate assembly patterns are allowed for certain operational areas. Future work is recommended to determine the effect of different lay patterns on operational performance.
- The laboratory fixture and procedure described herein can be used to evaluate new airfield mat joint designs for comparison to AM2. Friction stir welding techniques may be used to weld harder, but dissimilar, aluminum alloy end connectors to the main AM2 extrusion in attempt to improve joint fatigue resistance. The laboratory method is recommended for use to quantify improvements as a result of changing the material type or the design of new mat joints.
- The approach used to develop the laboratory low-cycle fatigue method described herein is recommended for consideration for other transportation structures installed over a deformable medium.

References

Ahlvin, R. G. 1991. *Origin of developments for structural design of pavements*. Technical Report GL-91-26. Vicksburg, MS: U.S. Army Engineer Waterways Experiment Station.

Allison, P. G., T. W. Rushing, and L. Garcia. 2014. *Analysis of lightweight materials for the AM2 system*. ERDC/GSL TR-14-18. Vicksburg, MS: U.S. Army Engineer Research and Development Center.

ASTM 2012. *Standard test method for strain-controlled fatigue testing*. ASTM E606/E606M. West Conshohocken, PA.

Azzam, D., and C. C. Menzemer. 2006. Fatigue behavior of welded aluminum light pole support details. *Journal of Structural Engineering* 132(12):1919-1927.

Berney, E. S., W. D. Hodo, and J. A. Vera. 2006. *Determination of unit section modulus for finite element modeling of matting systems*. ERDC/GSL TR-06-10. Vicksburg, MS: U.S. Army Engineer Research and Development Center.

Carr, G. L. 1972. *Evaluation of Kaiser XM19 waterproof aluminum honeycomb landing mat with D and D1 connectors*. Miscellaneous Paper S-72-4. Vicksburg, MS: U.S. Army Engineer Waterways Experiment Station.

Carr, G. L. 1973. *Evaluation of Goodyear medium-duty aluminum honeycomb landing mat*. Miscellaneous Paper S-73-8. Vicksburg, MS: U.S. Army Engineer Waterways Experiment Station.

Carr, G. L. 1974. *Engineer design test of modified XM19 special surfacing landing mat*. Miscellaneous Paper S-71-28. Vicksburg, MS: U.S. Army Engineer Waterways Experiment Station.

Chai, J., and N. Miura. 2002. Traffic-load-induced permanent deformation of road on soft subsoil. *Journal of Geotechnical and Geoenvironmental Engineering* 128(11):907-916.

Coughlin, R., and S. Walbridge. 2012. Fatigue testing and analysis of aluminum welds under in-service highway bridge loading conditions. *Journal of Bridge Engineering* 17(3):409-419.

Doyle, J. D., I. L. Howard, C. A. Gartrell, G. L. Anderton, J. K. Newman, and E. S. Berney IV. 2014. Full-scale instrumented testing and three-dimensional modeling of airfield matting systems. *International Journal of Geomechanics* 14(2):161-170.

Garcia, L., T. W. Rushing, and Q. S. Mason. 2014a. *AM2 25 CBR subgrade sensitivity test*. ERDC/GSL TR-14-7. Vicksburg, MS: U.S. Army Engineer Research and Development Center.

Garcia, L., T. W. Rushing, B. A. Williams, and C. A. Rutland. 2014b. *AM2 100 CBR subgrade sensitivity test*. ERDC/GSL TR-14-37. Vicksburg, MS: U.S. Army Engineer Research and Development Center.

Garcia, L. 2015. Full-scale instrumented evaluations of multiple airfield matting systems on soft soil to characterize permanent deformation. MS thesis, Mississippi State University.

Gartrell, C. A. 2007. *Full-scale instrumented testing and analysis of matting systems for airfield parking ramps and taxiways*. ERDC/GSL TR-07-33. Vicksburg, MS: U.S. Army Engineer Research and Development Center.

Gartrell, C. A., J. K. Newman, and G. L. Anderton. 2009. Performance measurements of pavement matting systems by full-scale testing over differing soil strengths. *Journal of Materials in Civil Engineering* 21(10):561-568.

Gonzalez, C. R., and T. W. Rushing. 2010. Development of a new design methodology for structural airfield mats. *International Journal of Pavement Research and Technology* 3(3):102-109.

Green, H. L. 1972. *Evaluation of Harvey aluminum 1- by 12-ft extruded light-duty landing mat with symmetrical butt-type end connectors*. Miscellaneous Paper S-72-38. Vicksburg, MS: U.S. Army Engineer Waterways Experiment Station.

Green, H. L., and C. T. McCormick. 1971. *Evaluation of Harvey aluminum 1- by 12-ft extruded light-duty landing mat with overlap/underlap end connectors*. Miscellaneous Paper S-71-29. Vicksburg, MS: U.S. Army Engineer Waterways Experiment Station.

Hambleton, J. P., and A. Drescher. 2008. Modeling wheel-induced rutting in soils: Indentation. *Journal of Terramechanics* 45:201-211.

Harr, M. E., and J. C. Rosner. 1969. *A theoretical study of landing mat behavior*. Contract Report S-69-7. Vicksburg, MS: U.S. Army Engineer Waterways Experiment Station.

Jogi, B. F., P. K. Brahmankar, V. S. Nanda, and R. C. Prasad. 2008. Some studies on fatigue crack growth rate of aluminum alloy 6061. *Journal of Materials Processing Technology* 201(1-3):380-384.

Jones, R., D. Horner, P. Sullivan, and R. Ahlvin. 2005. A methodology for quantitatively assessing vehicular rutting on terrains. *Journal of Terramechanics* 42:245-257.

Kaisand, L. R., and D. F. Mowbray. 1979. Relationships between low-cycle fatigue and fatigue crack growth rate properties. *Journal of Testing and Evaluation* 7(5):270-280.

Kawasaki, T., T. Makino, K. Masai, H. Ohba, Y. Ina, and M. Ezumi. 2004. Application of friction stir welding to construction of railway vehicles. *JSME International Journal Series* A 47(3):502-511.

Li, D., and E. Selig. 1996. Cumulative plastic deformation for fine-grained subgrade soils. *Journal of Geotechnical Engineering* 122(12):1006-1013.

Monismith, C. L., N. Ogawa, and C. R. Freeme. 1975. Permanent deformation characteristics of subgrade soils due to repeated loading. *Transportation Research Record; Journal of the Transportation Research Board* 537:1-17.

Pickett, G. 1951. *Analytical studies of landing mats for forward airfields: Final report to Corps of Engineers*. Vicksburg, MS: U.S. Army Engineer Waterways Experiment Station.

Pickett, G. 1955. *Analytical studies of orthotropic landing mats for forward airfields*. Misc. Paper 4-113. Vicksburg, MS: U.S. Army Engineer Waterways Experiment Station.

Rodriguez, R. I., J. B. Jordon, P. G. Allison, T. Rushing, and L. Garcia. 2015. Microstructure and mechanical properties of dissimilar friction stir welding of 6061-to 7050 aluminum alloys. *Material and Design* 83:60-65.

Rodriguez, R. I., J. B. Jordon, P. G. Allison, T. Rushing, and L. Garcia. 2016. Low-cycle fatigue of dissimilar friction stir welded aluminum alloys. *Material Science and Engineering A* 654:236-248.

Rushing, T. W., and J. S. Tingle. 2007. *AM2 and M19 airfield mat evaluation for the rapid parking ramp expansion program*. ERDC/GSL TR-07-5. Vicksburg, MS: U.S. Army Engineer Research and Development Center.

Rushing, T. W., N. Torres, and Q. S. Mason. 2008. *AM2 10 CBR subgrade sensitivity test for the parking ramp expansion program*. ERDC/GSL TR-08-13. Vicksburg, MS: U.S. Army Engineer Research and Development Center.

Rushing, T. W., and Q. S. Mason. 2008. *AM2 15 CBR subgrade sensitivity test for the rapid parking ramp expansion program*. ERDC/GSL TR-08-25. Vicksburg, MS: U.S. Army Engineer Research and Development Center.

Rushing, T. W., and I. L. Howard. 2011. Matting solutions for low-volume roads. *Transportation Research Record; Journal of the Transportation Research Board* 2204:92-101.

Rushing, T. W., and I. L. Howard. 2015. Prediction of soil deformation beneath temporary airfield matting systems based on full-scale testing. *Journal of Terramechanics* 58: pp 1-9.

Rushing, T. W., I. L. Howard, J. B. Jordon, and P. G. Allison. 2016. Laboratory characterization of fatigue performance of AM2 aluminum airfield matting. *Journal of Materials in Civil Engineering* 28(11). (DOI: 10.1061/(ASCE)MT.1943-5533.0001620).

Rushing, T. W., and I. L. Howard. 2017. Analysis of AM2 airfield matting performance under six-wheel Boeing C-17 gear loading. *Journal of Testing and Evaluation* 45(6). (DOI: 10.1520/JTE20160255).

Saleem, M., A. Mirmiran, J. Xia, and K. Mackie. 2012. Experimental evaluation of aluminum bridge deck system. *Journal of Bridge Engineering* 17(1):97-106.

Smith, C. J. 1972. *Evaluation of XM20 and XM20E1 landing mats under heavy-duty load*. Miscellaneous Paper S-72-39. Vicksburg, MS: U.S. Army Engineer Waterways Experiment Station.

U.S. Army Corps of Engineers. 1995. *Handbook for concrete and cement: Standard test method for determining the California bearing ratio of soils*. CRD-C 654-95. Vicksburg, MS: USACE.

Vahedifard, F., J. D. Robinson, G. L. Mason, I. L. Howard, and J. D. Priddy. 2016. Mobility algorithm evaluation using a consolidated database developed for wheeled vehicles operating on dry sands. *Journal of Terramechanics* 63(Feb):13-22.

Vahedifard, F., J. M. Williams, G. L. Mason, I. L. Howard, and J. D. Priddy. 2017. Development of a multi-year database to assess off-road mobility algorithms in fine-grained soils. *International Journal of Vehicle Performance* 3(1):3-18.

White, D. W. Jr. 1971a. *Evaluation of Dow Chemical Company extruded aluminum two-piece 2- by 12-ft landing mat (MX18-D)*. Miscellaneous Paper S-71-28. Vicksburg, MS: U.S. Army Engineer Waterways Experiment Station.

White, D. W. Jr. 1972. *Evaluation of Dow Chemical extruded truss-web landing mat*. Miscellaneous Paper S-72-40. Vicksburg, MS: U.S. Army Engineer Waterways Experiment Station.

White, D.W. Jr. 1973. *Evaluation of Dow Chemical Company extruded aluminum 4-piece 4- by 4-ft landing mat (MX18-E)*. Miscellaneous Paper S-73-9. Vicksburg, MS: U.S. Army Engineer Waterways Experiment Station.

White, D. W. Jr. 1974. *Evaluation of Dow Chemical production extruded truss-web landing mat*. Miscellaneous Paper S-74-12. Vicksburg, MS: U.S. Army Engineer Waterways Experiment Station.

White, T. D. 1971b. *Theoretical landing mat analysis*. Miscellaneous Paper S-71-21. Vicksburg, MS: U.S. Army Engineer Waterways Experiment Station.

Zwerneman, F., and K. H. Frank. 1988. Fatigue damage under variable amplitude loads. *Journal of Structural Engineering* 114(1):7-83.

REPORT DOCUMENTATION PAGE

Form Approved
OMB No. 0704-0188

1. REPORT DATE *(DD-MM-YYYY)*	2. REPORT TYPE	3. DATES COVERED *(From - To)*
January 2018	Final Technical Report	

4. TITLE AND SUBTITLE

Performance Prediction Relationships for AM2 Airfield Matting Developed from Full-Scale Accelerated Testing and Laboratory Experimentation

5a. CONTRACT NUMBER

5b. GRANT NUMBER

5c. PROGRAM ELEMENT NUMBER

6. AUTHOR(S)

Timothy W. Rushing

5d. PROJECT NUMBER
Demonstration Project 63

5e. TASK NUMBER

5f. WORK UNIT NUMBER

7. PERFORMING ORGANIZATION NAME(S) AND ADDRESS(ES)

U.S. Army Engineer Research and Development Center
Geotechnical and Structures Laboratory
3909 Halls Ferry Road
Vicksburg, MS 39180-6199

8. PERFORMING ORGANIZATION REPORT NUMBER

ERDC/GSL TR-18-1

9. SPONSORING / MONITORING AGENCY NAME(S) AND ADDRESS(ES)

U.S. Air Force Civil Engineer Center
Tyndall AFB, FL 32403-5319

10. SPONSOR/MONITOR'S ACRONYM(S)

AFCEC

11. SPONSOR/MONITOR'S REPORT NUMBER(S)

12. DISTRIBUTION / AVAILABILITY STATEMENT

Approved for public release; distribution is unlimited.

13. SUPPLEMENTARY NOTES

14. ABSTRACT

The AM2 airfield matting system is used by the U.S. military for temporary, rapidly constructed airfields. Predicting the number of allowable aircraft passes across an AM2 installation is challenging because of the complex design of the joining system and the fatigue behavior of the joints. Prior to this work, the prevailing methods used to predict the performance of AM2 were based on the CBR design procedure for flexible pavements using a small number of full-scale test sections over CBRs ranging from 4 to 10 percent and simulated aircraft that are no longer in service. This report presents results from nine full-scale experiments conducted on sections of AM2 matting installed on un-stabilized soil and gravel subgrades with CBRs of 6, 10, 15, 25, and 100 percent, and provides improved relationships for predicting subgrade deformation underneath an AM2 mat installation and the associated fatigue damage when subjected to F 15E and C 17 traffic. Additionally, a laboratory fixture and procedure is described for evaluating an AM2 style joint in fatigue and relating its performance to given field conditions without requiring the expense of full-scale testing. These relationships are suitable for design and evaluation frameworks currently used for airfield pavements and matting systems.

15. SUBJECT TERMS

Runways (Aeronautics)—Evaluation, Landing mats—Fatigue, Pavements, Trafficability

16. SECURITY CLASSIFICATION OF:			17. LIMITATION OF ABSTRACT	18. NUMBER OF PAGES	19a. NAME OF RESPONSIBLE PERSON
a. REPORT	b. ABSTRACT	c. THIS PAGE			19b. TELEPHONE NUMBER *(include area code)*
UNCLASSIFIED	UNCLASSIFIED	UNCLASSIFIED	SAR	91	